

**Water-mediated adhesion of oil sands on solid surfaces at low
temperature and possible solutions to mitigate adhesion**

by

Qimeng Yang

A thesis submitted in partial fulfillment of the requirements for the degree of

Master of Science

in

Materials Engineering

Department of Chemical and Materials Engineering
University of Alberta

© Qimeng Yang, 2022

Abstract

Adhesion of frozen granular materials on solid surfaces creates various problems for surface cleaning, reduces the carrying capacity of vehicles, and increases energy consumption for in-land transportation. Here in the first part of this thesis, water content demonstrates to determine the adhesion strength of oil sands (a complex granular matter) on solid surfaces at temperature of $-2.5\text{ }^{\circ}\text{C}$ to $-20\text{ }^{\circ}\text{C}$. Measurements by X-ray micro-computed tomography revealed that water formed capillary bridges between the sand particles and the solid substrate and more air gaps at the interface between oil sands and the substrate are filled with interstitial water at a higher content. The minimal force required to push the frozen oil sands off the substrate was experimentally measured and the adhesion strength was identified to increase linearly with water content from 4 to 14 wt% on both rubber and steel substrate. For short freezing time at a fixed water content, lowering the temperature increased the adhesion strength on the steel substrate. Fouling from a layer of bitumen or asphaltenes aggravated the adhesion of oil sands on steel. A theoretical model was proposed to rationalize the linear relationship between water content and the adhesion strength, based on the contact area between ice and the substrate.

In the second main part of this thesis, the adhesion behavior of oil sands under more complicated conditions was studied. The dependence of the adhesion of oil sands on hydrophobicity and softness of the substrates was found to follow the same trend as the ice adhesion strength on both hard and soft substrates. The adhesion strength of oil sands were directly proportional to the ice adhesion strength on the substrate, confirming the significance of ice to the adhesion of frozen granular matrix.

Furthermore, the adhesion of oilsands on the substrate was found to increase with the load on the oilsands up to a plateau. The increase of adhesion strength with the load was attributed to the increase in water/ice contact area with the substrate under a higher load, and the plateau in adhesion strength may be explained by the fact that the void space in the oil sands granular matrix was limited by the packing mode.

Finally, the performance of various types of liquids including aqueous ethylene glycol solution as anti-freezing liquid by spraying each liquid on a target substrate was evaluated. We first established a simple method to spray coat a little amount of pure ethylene glycol on the substrate to dramatically decrease the oil sands adhesion strength. More types of the anti-freezing liquids were tested after we found the strategy worked well in reducing the oil sands adhesion. Also, the sprayed droplets were found to stay stable with time and under shearing force. The strategy of spraying anti-freezing liquids was proven to be applicable for the industrial scale as well. The approach proposed in this thesis work may reduce the energy consumption in transport and processing of wet granular materials, and potentially save manpower and the cost from cleaning in industrial operations. The insight from this thesis work may have wide applicability to many natural and industrial processes, such as soil formation, food processing and storage, and porous structures in ice crystal-templating nanomaterials synthesis by freezing-drying.

Preface

This thesis is an original work by **Qimeng Yang**. The chapters in this work contain modified sections of the two following works:

1. Work submitted under **Q. Yang**, J. B. You, B. Tian, S. Sun, D. Daniel, Q. Liu, X. Zhang. Water-mediated adhesion of oil sands on solid surfaces at low temperature, *Fuel*. (2021). I am the main author of this work and was responsible for collecting and analyzing the data and writing up the manuscript. J. B. You and D. Daniel are responsible for the construction of the adhesion strength measurement setup and give detailed comments and revisions to the manuscript. B. Tian and S. Sun are the stewards from Imperial Oil Ltd., Canada, providing the field data from the oil industry and helping to evaluate the feasibility of possible solutions to mitigate oil sands adhesion. Q. Liu is the co-supervisor of the project and was providing suggestions on revising the manuscript with his strong experience in the oil industry. And X. Zhang is the supervisory author contributing intellectually and were involved with the manuscript composition. Modified sections of this work were used in Chapter 1 and Chapter 3.
2. Manuscript under preparation by **Q. Yang**, N. Moradpour, J. B. You, D. Wang, X. Deng, B. Tian, S. Sun, Q. Liu, D. Daniel, X. Zhang. Effects of load and substrate properties on ice-enhanced adhesion of frozen oil sands. I am the main author of this work and was responsible for collecting and analyzing the data and writing up the manuscript. N. Moradpour is responsible for collecting part of the data for the manuscript and writing up the section of the influence from

the water contact angle on ice adhesion strength. J. B. You is responsible for the construction of the adhesion strength measurement setup and give comments and revisions to the manuscript. B. Tian and S. Sun are the stewards from Imperial Oil Ltd., Canada, providing the field data from the oil industry and helping to evaluate the feasibility of possible solutions to mitigate oil sands adhesion. Q. Liu is the co-supervisor of the project and was providing suggestions on revising the manuscript with his strong experience in the oil industry. D. Daniel is the co-supervisor for this project, who is responsible to give detailed comments and revisions to the manuscript. And X. Zhang is the supervisory author contributing intellectually and were involved with the manuscript composition. Modified sections of this work were used in Chapter 1 and Chapter 4. The supporting information of this manuscript is provided in Appendix A and Appendix B.

3. Patent filed under the title of ‘METHOD TO REMOVE OIL SANDS CONTAMINATION OF STEEL SURFACES’ proposed by X. Zhang, **Q. Yang**, Q. Liu, B. Tian, S. Sun. I’m one of the main contributors to this patent work and helped with writing up the patent file. And X. Zhang is the main contributor who collaborated with Imperial Oil Ltd. and University of Alberta to file the patent. Q. Liu is the co-supervisor of the project and was providing suggestions on revising the manuscript with his strong experience in the oil industry. B. Tian and S. Sun are the stewards from Imperial Oil Ltd., Canada, providing the field data from the oil industry and helping to evaluate the feasibility of possible solutions to mitigate oil sands adhesion provided in the patent.

Acknowledgements

First and foremost, I would like to express my sincere gratitude to my supervisors, Drs. Xuehua Zhang, Dan Daniel and Qi Liu. Thank you for your patience, support and wisdom shared with me throughout my graduate studies. Dr. Zhang provided me with the great opportunity to work as a researcher in the warmest group that I have ever been in. I still remembered the moment when Dr. Zhang accepted me as her student in the group. That was one of the best memories in my life time and I would always treasure this experience to work in the group of Soft Matter and Interfaces. Dr. Daniel is an excellent supervisor who is easy going and always have great inspirations in writing. Although due to the crisis of Covid-19, we did not get the chance to meet in person, I still learned a lot from him. Dr. Qi Liu always provided me insights from his background knowledge in the oil industry and polished my work.

I would also like to express my gratitude for the stewards of the project from Imperial Oil Ltd., Ms. Shaofeng Sun and Brianna Tian. With the monthly meeting with them, I learned a lot from the oil industry and got familiar with how the research study worked for the real industry.

I am also grateful to have worked with Dr. Jae B. You and Mrs. Nikoo Moradpour. Without their guidance, advice and support, this thesis work would not have been possible.

I would like to thank all the present and previous members of the Soft Matter and Interfaces group I had the opportunity to work with. I appreciate all the advice and support they provided me.

I would also like to acknowledge the financial support obtained from Institute for Oil Sands Innovation (IOSI) (project number IOSI 2019-11) and from the Natural Science and Engineering Research Council of Canada (NSERC).

To my parents, Xuan Yang and Donghong Liu. Thank you for always encouraging me to pursue my dreams. Without your love and constant support, this work would not have been possible.

Finally, to my girlfriend, Siyi Bian. Thank you for your patience, love and for always believing in me during such a difficult time with Covid crisis. Wish that we could have more time to share with each other after we fulfilled the dreams of both of us.

Table of Contents

1	Introduction	1
1.1	Background	1
1.1.1	Adhesion of frozen matter on solid substrates	1
1.1.2	Strategies for reducing ice adhesion strength	4
1.1.3	Spraying method for icephobic coatings	11
1.2	Motivation	12
1.3	Thesis Objectives	13
1.4	Thesis Outline	14
2	Methods and procedure	15
2.1	Methods and procedure for Chapter 3	15
2.1.1	Preparation and characterization of substrates	15
2.1.2	Preparation of oil sands samples	17
2.1.3	Micro-CT scanning of oil sands	17
2.1.4	Quantitative measurements of frozen oil sand adhesion	18
2.2	Methods and procedure for Chapter 4	20
2.2.1	Preparation of substrates	20
2.2.2	Spray coating and stability test of anti-freezing liquid	22
2.2.3	Procedure for large scale tests	23
3	Water-mediated adhesion of oil sands on solid surfaces at low temperature	25

3.1	Oil sands microstructure	25
3.2	Oil sands adhesion in the limit of short freezing time	28
3.3	Oil sands adhesion in the limit of long freezing time	32
3.4	Mitigation of oil sands adhesion on multiple substrates	33
3.5	Conclusions	34
4	Effects of load and substrate properties on ice-enhanced adhesion of frozen oil sands	35
4.1	Effects of surface properties on adhesion	36
4.2	Effects of load on oil sands adhesion strength	39
4.3	Mitigation of adhesion by anti-freezing liquid	41
4.4	Conclusions	45
5	Conclusions & Future Work	47
5.1	Main results and contributions	47
5.2	Future Work	48
	Bibliography	51
	Appendix A: DSC result of oil sands sample	59
A.1	Procedure of DSC tests	59
A.2	Results of DSC tests	59
	Appendix B: Influence of particle size on adhesion force of water-wet sands	61
B.1	Preparation of sample and procedure of adhesion force measurements	61
B.2	Results of sand adhesion force measurements	62

List of Tables

2.1	Contact angle of water on substrates	16
2.2	Composition of oil sands samples (wt%)	17
2.3	Contact angle of water and Young's modulus of substrates	22
3.1	Compositions of oil sand samples after compression at 60 <i>kPa</i> . <i>z</i> : the distance from the substrate.	27
3.2	Conditions and results of τ_{ad} ($C_w = 10$ wt%) measurement with EG spray measured after 5 <i>min</i> of freezing.	33
4.1	Conditions and results of τ_{os} measurement with anti-freezing liquid spray.	43

List of Figures

1.1	Photo of oil sands fouling on truck after dumping.	2
1.2	Effect of surface roughness and surface energy on the ice adhesion strength of soft coatings.	5
1.3	Effect of shear modulus of the soft coatings on ice adhesion strength .	6
1.4	Effect of coating thickness on the ice adhesion strength of soft coatings	8
1.5	Mechanism of self-lubricating coating for icephobic purpose.	10
2.1	Adhesion strength measurement device and test procedure.	19
2.2	Schematic of large scale test procedure with the glycol spray.	24
3.1	Micro-CT scanning image of oil sands and model of oil sands.	26
3.2	Effect of water content ($C_w = 4$ to 14 wt%) on τ_{ad} at temperature from -2.5 °C to -20 °C.	28
3.3	Effect of temperature on τ_{ad} and correlation of nucleation rate J with τ_{ad}	31
3.4	Equilibrium τ_{ad} after longer freezing time.	32
4.1	Effect of substrate surface properties on ice/oil sands adhesion strength on hard (Silicopon, CCO, and steel) and soft substrates (rubber, PDMS, and structured PDMS).	37
4.2	Effect of load on the τ_{os}	39
4.3	Representative force curves for oil sands adhesion strength on steel/oil sands fouled layer with/without glycol spray (EG:water = 2:1).	42

4.4	Volume change and lateral-view images of EG spray (EG:water = 2:1) droplets on steel substrate.	43
4.5	Effects of EG spray (EG:water = 2:1) on reducing oil sands adhesion at large scale.	44
A.1	DSC result of oil sands sample with 4 and 10 wt% of water.	60
B.1	Results of adhesion force measurements for wet sands sample.	62

List of Symbols

A	Pre-exponential factor for Arrhenius equation
A_{ice}	Surface coverage of ice
C	Constant for water nucleation
C_w	Water content by weight
F_p	Pinning force per unit length
F_{ad}	Detaching force
J	Nucleation rate
K_B	Boltzmann's constant
L_v	Specific latent heat of fusion for ice.
P_s	Shear strength of adhesion
R	Work of detachment of water
T_m	Melting point of ice
ΔG	Activation energy for nucleation
ΔS	Entropy of fusion
ΔT	Degree of supercooling
γ	Surface tension
γ_{LV}	Liquid-vapour interfacial tension

τ_{ad}	Adhesion strength
τ_{ice}	Adhesion strength of ice
τ_{os}	Adhesion strength of oil sands
θ_{adv}	Advancing contact angle of water
θ_{rec}	Receding contact angle of water
$f(\theta)$	Geometrical factor
$t_{plateau}$	Freezing time for τ_{os} to reach plateau
z	Distance of the sample from the substrate

Abbreviations

CAH Contact angle hysteresis.

CCO Chromium carbide overlay.

CT Computed tomography.

DSC Differential scanning calorimetry.

EG Ethylene glycol.

F Fluoridated silicone coating.

G Traditional silicone coating.

H-PDMS Hydrogen-terminated PDMS.

NMR nuclear magnetic resonance.

NP Nanoparticles.

PDMS Polydimethyl siloxane.

PEG Polyethylene glycol.

PG Propylene glycol.

PSBMA Polysulfobetaine methacrylate.

RPM Revolution per minute.

Silikopon Silikopon EF, a type of silicone-epoxy hybrid material.

SLIPS Slippery liquid infused porous surface.

v-PDMS vinyl-terminated PDMS.

XRD X-ray diffraction.

Chapter 1

Introduction

1.1 Background

1.1.1 Adhesion of frozen matter on solid substrates¹

Freezing of wet granular materials is important for many processes, ranging from landscape and soil formation in nature[1], to food storage in cold chain[2, 3], preservation of biological materials and systems at low temperature[4], and porous materials synthesis by templating ice crystals [5]. Phase change of interstitial water trapped in confined spaces plays an essential role in all the above processes. For instance, the cycles of freezing and thawing of water determines weathering of rocks in soil formation [6]. In food processing, the texture of ice creams is strongly correlated with ice crystals in the matrix of fat, proteins, and bubbles [7]. Ice nucleation and sublimation in a freezing-drying process creates porous structures in the framework of materials, producing not only soft porous polymers like hydrogels or aerogels, but also hard materials of ceramics, metal or metal organic frameworks [5].

As a complex granular matrix in the nature, oil sands typically consists of 80 to 90 wt% sand (including silica, clay, and other minerals), 8 to 13 wt% of bitumen (saturates, aromatics, resins, and asphaltenes) [8, 9], and 2 to 8 wt% of water[9–

¹This section contains modified parts of 1) submitted work **Q. Yang**, J. B. You, B. Tian, S. Sun, D. Daniel, Q. Liu, X. Zhang. Water-mediated adhesion of oil sands on solid surfaces at low temperature, *Fuel*. (2021) and 2) manuscript under preparation by **Q. Yang**, N. Moradpour, J. B. You, B. Tian, S. Sun, D. Daniel, Q. Liu, D. Wang, X. Deng, X. Zhang. Effects of load and substrate properties on ice-enhanced adhesion of frozen oil sands.

12]. Strong adhesion of oil sands to the surface of truck bed and canopy causes serious fouling problems in the oil industry. As shown in Figure 1.1, the adhered oil sands reduces transport capacity of the trucks, consumes excess amount of fuels to transport the carryback after dumping, requires cleaning processes by steaming or manual shoveling. The fouling issue appears to be more serious in winter than in warmer seasons. The estimated cost is several million dollars per year for one fleet working on the mining site. Therefore, it is important to understand the mechanism behind the strong adhesion of oil sands at low temperature, and identify potential approaches for mitigation.



Figure 1.1: Photo of oil sands fouling on truck after dumping. Taken from a mining site.

Our recent work showed that at the temperature below the freezing point of water, the adhesion of oil sands increased rapidly, and the adhesion strength of oil sands was strongly correlated to the water content. This drove us to recognize that ice may be the key factor that leads to the strong adhesion of oil sands after frozen. And studying the adhesion strength of ice can possibly be beneficial to reduce the adhesion of frozen oil sands. For ice accumulated on a solid surface, the physical and chemical properties of the solid substrate determine the adhesion strength [13–15]. On flat surfaces, Meuler et al [16] (and others[17–19]) showed that the ice adhesion strength is linearly proportional to the Young-Dupre work of adhesion $\gamma (1 + \cos \theta_{rec})$, where γ is the surface tension of water and θ_{rec} is the receding contact angle.

Increasing surface roughness can either decrease ice adhesion by trapping air pockets between ice and the surface[20] or increase adhesion by providing more sites for the nucleated ice to mechanically interlock with the substrates[21–25]. The discrepancy between advancing and receding contact angles, known as contact angle hysteresis (CAH), was also reported to influence the ice adhesion strength. CAH originates from the physicochemical and geometrical heterogeneities that disrupt the three-phase contact line movement. Higher hysteresis reflects greater extent of heterogeneities such as surface roughness or flexibility and chemical interactions [26–28]. It is worth to mention that for a substrate containing roughness or defects with opposite wettability, the adhesion of water droplets to the substrates could be higher, and thus increase the ice adhesion strength after frozen[29, 30].

When contacting a metal or a dielectric material, electrostatic force is the main contributor to ice adhesion [14, 31–35]. For surfaces with hydroxyl groups, hydrogen bonding between ice and substrate dominates, with insignificant contribution from van der Waals’ interactions[36–39]. Adding surfactants (such as polyglycerol to water) can reduce the ice adhesion strength, as the surfactants absorb onto the surface (such as copper) and reduce the work of adhesion[40, 41].

For freezing in porous structures formed by packed solid particles, water is typically classified into 3 categories: (1) free water (almost the same as bulk water); (2) slightly bound water that freezes at temperature slightly below the freezing point of water (0 °C); (3) strongly bound water that does not freeze even at -100 °C. The freezing point of water in confined space is determined by the size and shape of the pores, based on surface thermodynamics on microscopic scale [42]. When the pore size decreases, the expected freezing point of pore water also decreases. For example, the freezing point of water in porous silica glass was estimated to decrease from -1 °C to -9 °C when the pore size ranged from 1 to 0.01 μm [43].

In the mixtures of solid particles and two immiscible fluids, capillary network forms between the particles in suspension [44]. Depending on the fraction of liquid wetting

the particle surface, the mixture is stabilized in a pendular or capillary state. However, whether the capillary bridges of interstitial water correlates with the adhesion of granular materials on solid surfaces remains unclear.

1.1.2 Strategies for reducing ice adhesion strength

Soft coatings

The softness of the solid substrate is reported to decrease the ice adhesion strength. The difference in the stiffness between ice and a soft substrate leads to stress concentration at the ice-substrate interface, which facilitates the ice to detach from the the substrate by creating cracks at the interface under the shearing stress[45, 46]. The reduced adhesion strength was only valid when shearing stress is asserted on the ice adhered to the substrate. Among the candidate materials for soft coatings to achieve low ice adhesion, poly(dimethylsiloxane) (PDMS) – a silicone-based elastomeric polymer – has been studied the most, due to its natural hydrophobicity and tunable mechanical properties[47–50].

To figure out the mechanism of the ice-repellent property of the silicone-based soft coatings, Fu et al.[20] studied the effect of surface energy and surface roughness on the ice adhesion strength. In Figure 1.2 (a) & (b), we could see the surface roughness of both normal silicone coating (denoted as ‘G’, with surface energy of $\sim 62 \text{ mJ/m}^2$) and fluoridated silicone coating (denoted as ‘F’, with a surface energy of $\sim 12 \text{ mJ/m}^2$) increased with decorating by hydrophobic silica nanoparticles. The surface energy of the fluoridated silicone coating was naturally lower, and so as to the silica nanoparticles decorated ones. From Figure 1.2.(c) & (d), we could readily see the ice adhesion strength was constantly lower on fluoridated silicone coating, which possessed intrinsically lower surface energy. Increasing the surface roughness is beneficial to anti-icing performance for silicone coating with low surface energy, while simply making the silicone-based coating rougher will only cause stronger mechanical interlock between ice and the coating, leading to higher ice adhesion on normal silicone

coating shown in Figure 1.2.(c).

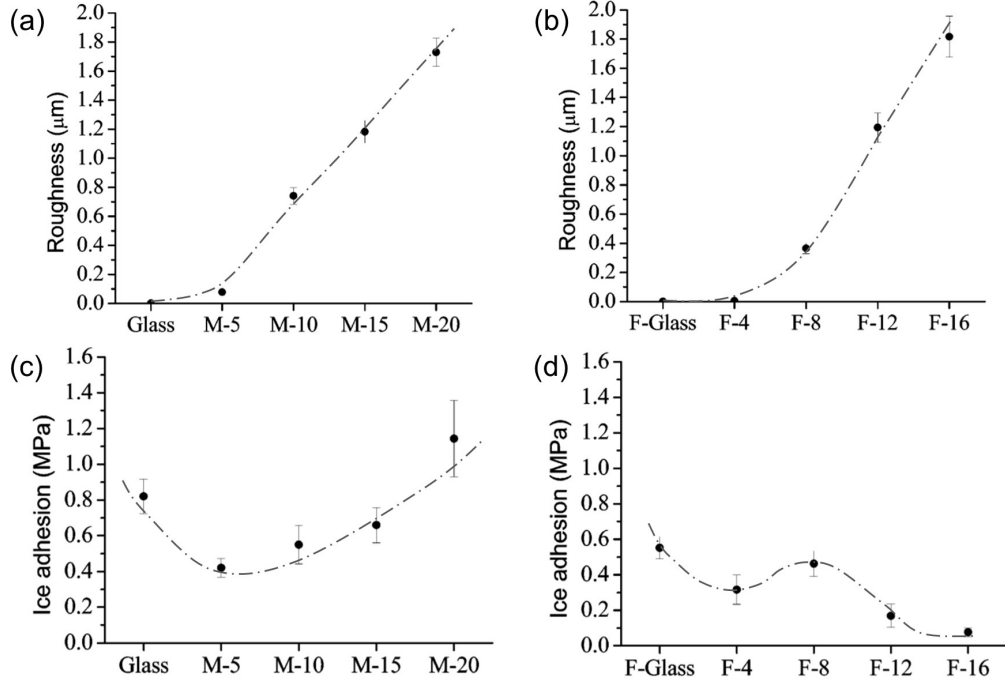


Figure 1.2: (a,b) - Effect of introducing hydrophobic silica particles on traditional silicone coating on glass(denoted as ‘G’, with surface energy of $\sim 62 \text{ mJ/m}^2$)/fluoridated silicone coating on glass(denoted as ‘F’, with a surface energy of $\sim 12 \text{ mJ/m}^2$) on the surface roughness of the substrates. The number beside represents the weight content of silica nanoparticles grafted into the silicone-based coating; (c,d) - Ice adhesion strength on silica nanoparticles decorated silicone coating/fluoridated silicone coating. The figure was modified from the work by Fu et al.[20]

Apart from surface energy and roughness, Golovin et al. demonstrated that, regardless of material chemistry, silicone-based soft coatings with low cross-linking density are efficient in reducing the ice adhesion. When the cross-linking density of a coating is low, it can induce interfacial slippage against ice, which significantly lowers the ice adhesion. Based on this idea, the authors achieved a minimum ice adhesion of $\tau_{ice} = 0.2 \text{ kPa}$ [51], which is much lower compared with the conventional superhydrophobic surface with ice adhesion of $\tau_{ice} \sim 100 \text{ kPa}$.

Unlike hard coating, where the receding water contact angle was reported to determine the ice adhesion strength on smooth surfaces,[16] the ice adhesion on soft PDMS coatings was later found to be dominated by its mechanical properties[46].

Since people found that the cross-linking density and the elastic/shear modulus of the soft coatings can be tuned by the ratio of elastomer base to curing agent[48], the ice adhesion on PDMS coatings is reported to increase linearly with the elastic/shear modulus of the coating, as shown in the Figure 1.3:

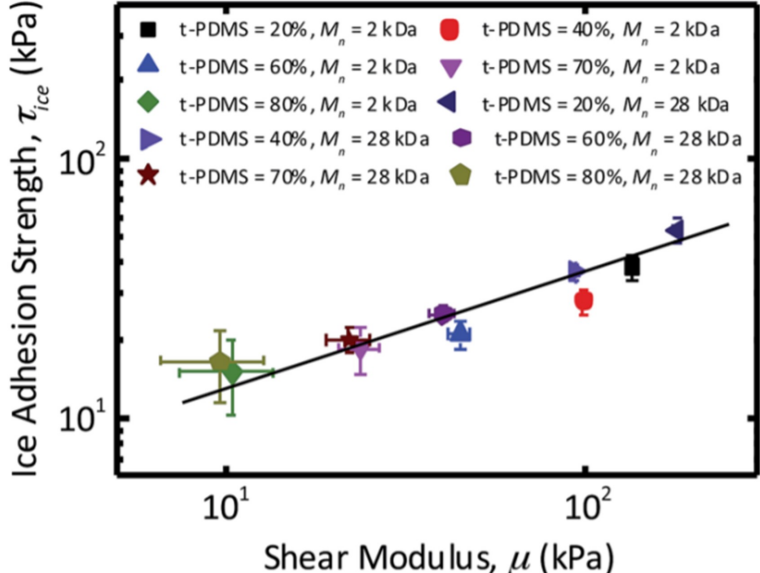


Figure 1.3: Effect of shear modulus on ice adhesion strength of a group of PDMS-based soft coatings. The figure was modified from the work of Beemer et al.[49]

As shown in Figure 1.3, Beemer et al. reported a PDMS gel synthesized by hydrosilylation of vinyl-terminated PDMS (v-PDMS) with H-terminated PDMS (H-PDMS) has a ice adhesion strength linearly related with the shear modulus of the coating.[49] The authors also tuned the cross-linking density of the gel by adding trimethyl terminated PDMS (t-PDMS) at varying proportions. The gel showed an optimized performance of ice-adhesion strength of $\tau_{ice} = 5.2$ kPa, which is significantly lower than a commercially available de-icing coating (NuSil R2180) with $\tau = 37$ kPa. In a later work, the same authors reported that soft PDMS can mitigate ice formation in conditions pertinent to aircraft during flight.[52] The authors attribute the excellent icephobic property on both the hydrophobic property of PDMS gel as well as its softness, which play a key role in bouncing off droplets that can accumulate on the surface and become ice.

The thickness of the soft coatings has also been reported as an important factor that influences the ice adhesion on soft coatings. Demonstrated by Wang et al.,[48] ice adhesion strength on PDMS coating has a linear relationship with the thickness of the coating to the power of -0.5 in Figure 1.4.(a). They attributed this trend with a finding from a previously published work by Kendall et al.[53] From the model proposed by Kendall et al., the tensile adhesion strength of a rigid solid to a soft elastomer has a linear relation with thickness to the power of -0.5. Because the tensile and the shear modulus of soft polymers are also linearly related[48], they rationalized the finding between ice adhesion strength and the coating thickness ($P_s \propto \text{thickness}^{-0.5}$). However, when the thickness of the coating reached a certain value, the influence from the coating thickness on ice adhesion was negligible, as shown in Figure 1.4.(b).

Apart from the outstanding mechanical property and the relatively low surface energy that makes silicon-based polymers promising for icephobic purpose, the abundant space between the polymer network and high affinity to oils with similar structures also endow the silicon-based coatings a possibility to be developed as liquid-infused surfaces to enhance the ice repellency. Due to the similarity in the molecular structure of silicon oil and silicon-based polymer, silicon oil is considered to be a very good candidacy for lubricating PDMS-based substrate to reduce the ice adhesion force by forming a oil-lubricated layer. If the lubrication layer is thick enough, interfacial slippage can also be achieved and thus dramatically decrease the ice-adhesion force. In a popular research, Zhu et al. introduced a PDMS-based coating infused with silicon oil and with addition of silica-nanoparticles to enhance the mechanical property and durability[54]. Surface modified nano-sized silica particles (primary size: 10-15 nm) were added to enhance the mechanical property and platinum catalyst was added to promote cross-linking between vinyl and silane group so that the silicon oil can be held in the polymer network.

Except for silicon oil that has almost the same structure as PDMS base, paraffin oil

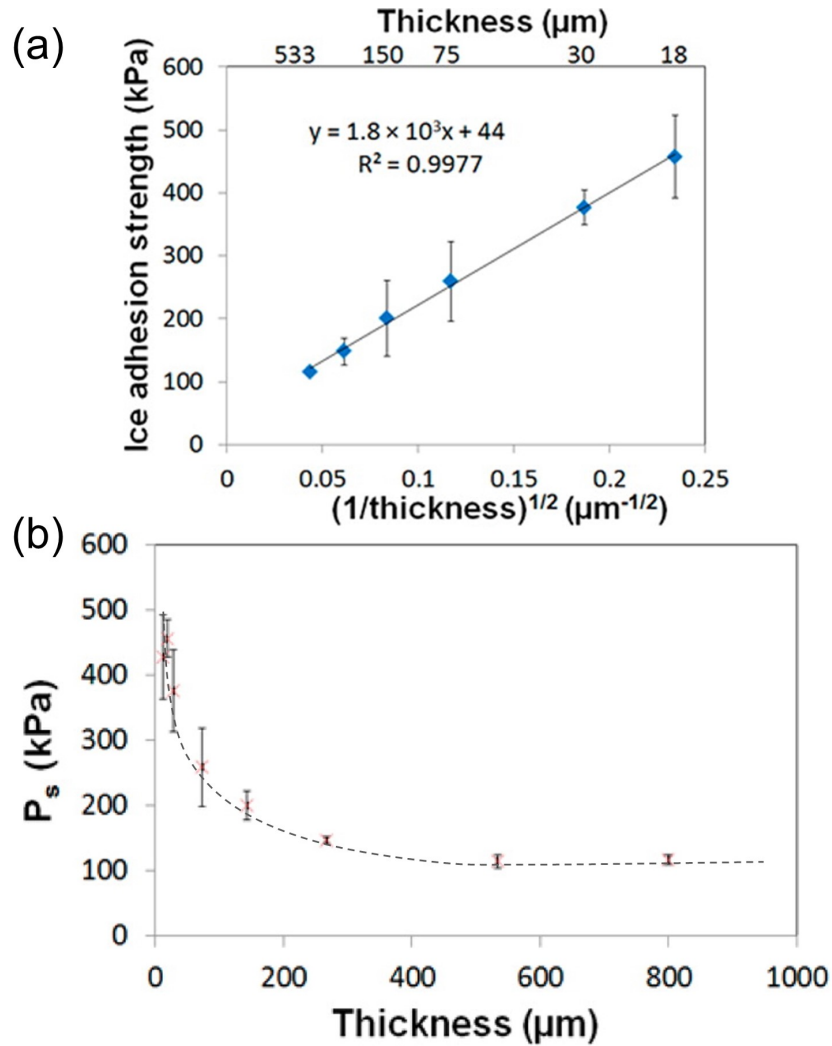


Figure 1.4: (a) - Linear relationship between ice adhesion strength and the thickness of PDMS coating by the power of 0.5 within the thickness of around 20-500 μm ; (b) - Relationship between ice adhesion strength and coating thickness from 20 to 800 μm . The figures were modified from the work by Wang et al.[48]

is another lubricate that can be infused into PDMS network to reduce ice adhesion. Wang et al. introduced an organogel system comprised of paraffin oil infused PDMS as anti-icing coating[55]. As they stated, organogel outperforms traditional lubricated surfaces in outdoor anti-icing application because of the nature for slow and continuous releasing of liquids from the three-dimensional polymer network, which is the main characteristic of an organogel system. Ice adhesion was found to be ultra-low - only 1.7 kPa even under extremely low temperature (-70 $^{\circ}\text{C}$). However, because of

the inevitable depletion of lubricant oil with icing/deicing cycles and the complicated procedure to refill lubricants into PDMS base, the research of oil-infused PDMS was only limited to lab scale and not applicable to industrial applications[56]. In this case, the study of self-lubricating coatings that could use surface non-freezing water as lubricant liquid brought the attention of many research groups.

Self-lubricated coatings

Since slippery liquid infused porous surface (SLIPS) as icephobic surfaces has been an attracting topic for many groups focusing on anti-icing surfaces, surface non-freezing water was seen as a promising candidate for the purpose of anti-icing, and this strategy was known as ‘self-lubricating coating’. The mechanism of self-lubricating coating was introduced in the work of Chen et al. that the hygroscopic polymer layer could serve as a reservoir to grab water from the surroundings and break the hydrogen bonds between water molecules near the surface. [57] Thus, the interfacial water close to the substrate could remain in liquid state and work as lubricant even below the freezing point of bulk water in nature (0 °C). Since the liquid-like surface could greatly reduce the attachment of ice, self-lubricating SLIPS, especially those with significant durability, is under extensive investigation for mitigating ice adhesion.

As described in Dr. Lei Jiang’s group[58], they successfully prepared a self-lubricating robust anti-icing surface on silicon wafer. They first etched some holes on silicon wafer and then introduced crosslinked hydrogel inside the as prepared pits. The hydrogel will bump out of the pits and form a self-lubricate layer on top of the wafer after condensation and perhaps deliquesces, and they will merge under molecular interactions. The self-lubricating layer can self-heal and could absorb water from the ice formed on top of that, and the reduced ice point on the layer can be attributed to the tuned water activity. While, in another work of the same group[59], they mentioned a new structure of anti-icing surface with grafted ionize polymer a hydrophobic polyurethane core. The hydrophilic corona structured self-lubricating

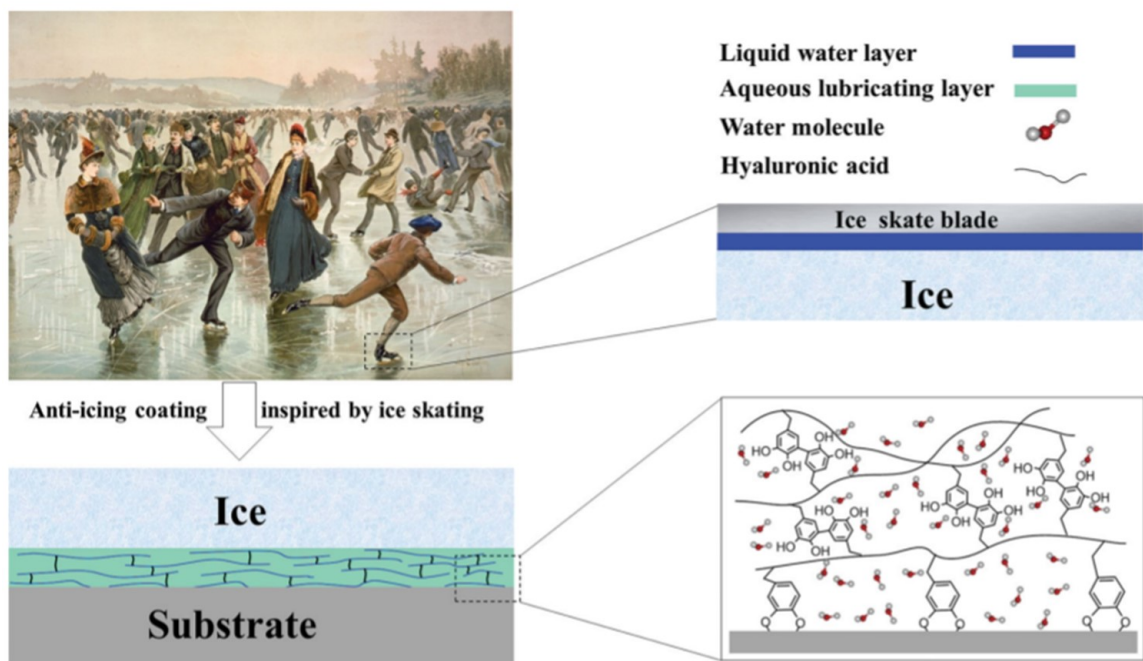


Figure 1.5: Mechanism of self-lubricating coating for icephobic purpose. Figure modified from the work of Chen et al.[57]

unit can be easily attached to a variety of substrates with the help of highly adhesive polyurethane core and thus induce the anti-icing performance on the surfaces attached by the units.

Also, in the work from Cao et al.[60], they mentioned that the addition of hydrophobic polymer into the polymer chain will enhance the performance of hydroscopic polymer PSBMA by dispersing water and facilitate the water absorption process. The similar strategy can be seen in many other works, such as the work from Chen et al.[61], who fabricated an amphiphilic copolymer made of PDMS and PEG. The slippery PDMS could facilitate the separation of formed ice layer and the bonded non-freezing water lubricate. The function of PEG is just like PSBMA, which is absorbing water from surroundings and form hydrogen bonding with water molecules to decrease its ice point. The PDMS-co-PEG system was applied to PDMS, epoxy and polyurethane base to show a significant reduction in the ice adhesion strength. However, since the preparation methods of self-lubricating layers were too compli-

cated and the price of the materials was typically high due to the requirement of co-polymerization, the application of self-lubricating polymer to the real industry was also restricted.

1.1.3 Spraying method for icephobic coatings

One critical issue that prevents putting icephobic coatings into real applications is the coating method. In laboratory researches, multiple-step coating methods (spin coating, dip coating, annealing/heat treatment, addition of nanoparticles) are commonly used. Also, the fabrication of fancy icephobic coatings usually contains surface micro/nano-structure or lubrication. However, these complicated fabrication methods are not possible to be applied to industrial applications due to the lack of experimental environments or the high cost. Compared with the fabrication methods mentioned above, one-step spray-coating method has an outstanding versatility and easiness to apply, enabling this method to be adopted to the fabrication of large-scale icephobic coating.

Sprayable silicone-based hydrophobic coatings

Silicon-based polymers were introduced in previous section to serve as a good candidate for icephobic coatings. However, the methods of preparing those silicon-based coatings, mainly PDMS-based coatings, are spin coating or dip coating, which are limited to small scale or highly dependent on the geometry of the substrate. In this section, a type of sprayable PDMS-based coating with superhydrophobicity and self-healing property is introduced.

As stated by Yao et al.[62], the sprayable hydrophobic PDMS-based coating they developed recently is promising to be used as anti-icing surfaces. The coating they developed is a kind of supramolecular material, which could have integrated properties of intrinsic healing, malleability, and recyclability. This can be attributed to the stable mechanical strength via reversible crosslinks. In their following work,

they introduced how they transferred the supramolecular silicon into sprayable superhydrophobic coating[63]. According to the authors, the polymeric coating they fabricated, with combined properties of superhydrophobicity, strong adhesion to substrates, mechanical robustness, and damage healing is of great importance for industries such as liquid transportation, oil-water separation, and anti-icing purpose. The main component of the coating is the same as what they mentioned in their previous work[62] and they also added silica nanoparticles to enhance the durability of the coating. Once sprayed on a porous substrate, the water contact angle can reach $157.2\pm 1.9^\circ$, and the water sliding angle can be as low as $7.8\pm 0.8^\circ$. The coating could recover from knife cutting tests for 10 times and tape peeling/sandpaper testing for over 100 times, demonstrating good durability.

1.2 Motivation

Among granular matters in nature, oil sands have complex compositions, typically consisting of 80 to 90 wt% sand (including silica, clay, and other minerals), 8 to 13 wt% of heavy oil bitumen (saturates, aromatics, resins, and asphaltenes) [8, 9], and 2 to 8 wt% of water[9–12]. Oil sands is an importance source of crude oil in Canada, since bitumen can be separated from solids by warm water extraction in surface mining operations [10, 11]. Strong adhesion of oil sands to steel substrates at low temperature creates problems for mining fleet management. The large carryback of oil sands after unloading reduces the transport capacity of the trucks moving from the mining point to the refinery station and causes extra time and cost for removing oil sands deposits from the truck surface. One may intuitively attribute adhesion of oil sands to heavy species in bitumen, in particular asphaltenes that are well-known to ‘glue’ firmly onto almost all kinds of solid surfaces, due to strong $\pi - \pi$ interactions and colloidal aggregation[64]. However, it was yet reported in the literature that what caused the strong adhesion of oil sands to steel substrates under 0°C . Moreover, there is no current commercially available methods to reducing the adhesion of frozen oil

sands to the steel substrates in winter. This work aims to not only figure out the mechanism of oil sands adhesion at low temperature, but give feasible and simple approach to solve the issue for the oil industry.

1.3 Thesis Objectives

The overall goal of this thesis is to investigate the factors that determined the adhesion strength of oil sands to the solid substrates, analyze the relationship between the composition and the adhesion strength of frozen oil sands, and provide solutions to mitigate the adhesion strength of oil sands with easy manners. The individual objectives of this thesis work are as following:

1. To observe the structure of oil sands with the help of micro-CT and figure out the relationship between changing the composition of oil sands and the contact area of each component at the oil sands-substrate interface.
2. To determine and analyze the reason for the correlation between the water content in oil sands and the adhesion strength of frozen oil sands to steel substrate.
3. To analyze the relationship between freezing temperature and oil sands adhesion strength with nucleation theory.
4. To evaluate the oil sands adhesion strength on substrates with different Young's modulus and surface wettability and relate oil sands adhesion with ice adhesion strength on the substrates.
5. To evaluate and analyze the influence from load on the oil sands sample to the adhesion strength of oil sands and give possible explanation.
6. To test the performance of anti-freezing liquid spray for reducing the adhesion strength of frozen oil sands on multiple substrates, evaluate the stability of the spray, and check if the spray works for large scale applications.

1.4 Thesis Outline

Chapter 1 provides a brief introduction on the adhesion of frozen matters to solid substrates, the possible mechanisms for the adhesion, and strategies to reduce the adhesion strength of ice studied in literature. The method of spray coating of the protective coatings to substrate to reduce the adhesion is also briefly discussed. The motivation and objectives of the thesis are also introduced in this chapter.

Chapter 2 provides the experimental procedures, equipment and characterization methods used to obtain the results given in Chapter 3 and Chapter 4.

Chapter 3 demonstrates the influence from water content on oil sands adhesion strength and a model of the oil sands, which is verified with the characterization of micro-CT system. The influence from freezing temperature and freezing time is also analyzed in this chapter. A possible solution to mitigate the adhesion of oil sands by spray coating of anti-freezing liquid is proposed and the performance of some preliminary tests with one type of anti-freezing liquid is presented.

Chapter 4 presents the experimental results and discussions for the study about the influence from substrate surface properties on oil sands adhesion strength. The correlation between ice adhesion strength and oil sands adhesion strength is demonstrated, and the influence from load on the adhesion strength is investigated. The performance of spraying of anti-freezing liquid with multiple composition is evaluated comprehensively. The stability of the spray is tested, and the results of the performance of the spray at a large scale are presented.

Chapter 5 summarizes the two works discussed in Chapter 3 and chapter 4 and finalizes with potential future works that could help determine the factors influencing the adhesion strength of oil sands and understand the ice nucleation process in granular matrix.

Chapter 2

Methods and procedure¹

2.1 Methods and procedure for Chapter 3

2.1.1 Preparation and characterization of substrates

Calibration of the device for adhesion strength measurements was performed by using a slab of polydimethylsiloxane (PDMS), as ice adhesion on PDMS has been extensively studied in literature. [46–49, 65] To fabricate the PDMS slab, a base and a curing agent (Sylgard 184, Dow Corning) were mixed rigorously at a weight ratio of 10:1 and cast onto a clean glass slide ($70\text{ mm} \times 20\text{ mm}$) to fully cover the slide surface. After degassing in vacuum for 30 minutes, the glass slide coated with PDMS resin was transferred into an oven to cure at $80\text{ }^\circ\text{C}$ for 2 hours. The thickness of the PDMS slab formed on the glass slide was around 1 mm . Before use, the PDMS slab was rinsed with acetone (>99.5%, Fisher), ethanol (>99%, Fisher), and deionized water. Reagents (acetone and ethanol) were used as received without any further treatment.

Two solid substrates were used for oil sands adhesion strength (τ_{ad}) measurements: stainless steel 304 (McMaster-Carr, USA) with thermal conductivity of 14 to 15 W/m.K [66, 67] and oil-resistant Buna-N nitrile rubber (McMaster-Carr, USA) with

¹This section contains modified parts of 1) submitted work **Q. Yang**, J. B. You, B. Tian, S. Sun, D. Daniel, Q. Liu, X. Zhang. Water-mediated adhesion of oil sands on solid surfaces at low temperature, *Fuel*. (2021) and 2) manuscript under preparation by **Q. Yang**, N. Moradpour, J. B. You, B. Tian, S. Sun, D. Daniel, Q. Liu, D. Wang, X. Deng, X. Zhang. Effects of load and substrate properties on ice-enhanced adhesion of frozen oil sands.

Table 2.1: Contact angle of water on substrates

Substrate	Advancing angle ($^{\circ}$)	Receding angle ($^{\circ}$)	Hysteresis ($^{\circ}$)
Stainless steel	92 ± 2	21 ± 4	71
Rubber	109 ± 3	58 ± 3	51
Bitumen-coated steel	102 ± 3	43 ± 4	51
Asphaltene-coated steel	96 ± 2	55 ± 4	41

thermal conductivity of around 0.25 W/m.K [68, 69]. The steel and rubber substrates were cut into square-shaped plates with the dimensions of $40 \text{ mm} \times 40 \text{ mm}$, and a thicknesses of 0.76 and 1.6 mm , respectively. The substrates were rinsed consecutively in acetone, ethanol, and water to clean the surface thoroughly before each experiment.

To simulate the industrial scenario where substrates are commonly fouled by bitumen and asphaltene in oil sands, the steel substrate was coated with bitumen/asphaltene. Bitumen used in this study was provided by an oil sands operator in northern Alberta, while n-pentane precipitated asphaltene was supplied by Quadris Canada Corporation. Bitumen and asphaltene were first dissolved in toluene ($>99.5\%$, Fisher) to achieve the same concentration of 250 mg/mL , and were homogenized by sonicating the solution for 15 min . To coat the steel, 0.75 mL of the bitumen or asphaltene solution was deposited on a steel plate, which was then spun at 600 revolutions-per-minute (RPM) for 30 sec on a spin coater (WS-650Mz, Laurell, USA). After spin coating, the coated substrates were placed under ambient condition for 2 days to ensure complete evaporation of the solvent. The coated substrates were rinsed with water before use. The thicknesses of the bitumen and asphaltene coatings were determined to be $30\text{-}50 \text{ }\mu\text{m}$ as measured by using an optical microscope.

The contact angles of water on the substrates were determined by using a contact angle instrument (DSA100 system, Kruss, USA). The advancing and receding contact angles of water are shown in Table 2.1.

Table 2.2: Composition of oil sands samples (wt%)

Water	Bitumen	Solids
4.0	13.0	83.0
6.0	12.7	81.3
8.0	12.5	79.5
10.0	12.2	77.8
12.0	11.9	76.1
14.0	11.6	74.4

2.1.2 Preparation of oil sands samples

Oil sands, which were provided by the same operator as the one for our bitumen sample, were homogenized and stored in sealed plastic bags at $-18\text{ }^{\circ}\text{C}$ to keep the samples consistent for all the experiments. Before use, the sample was thawed at room temperature overnight. The composition of the oil sands samples was determined by a set of standard Dean-Stark apparatus, under the standard procedure in literature[11, 70]. The samples used in this study naturally contained 4 wt% of water, 13 wt% of bitumen and 83 wt% of solids. To prepare oil sands with higher water weight percentage (C_w), a certain volume of deionized water was added with micro-pipettes and homogenized manually. To prevent water evaporation, the prepared samples with certain water contents were sealed with a paraffin film till the measurements. The composition of the oil sands used in this study is shown in Table 2.2.

2.1.3 Micro-CT scanning of oil sands

To evaluate the microstructures of oil sands, we scanned the samples with C_w of 4 and 14 wt%. An X-ray micro-CT system (ZEISS Xradia Versa 620 X-Ray Microscope, Zeiss, Germany) was used and the CT scans were performed under ambient condition. Around 0.3 g of oil sands were confined in a polypropylene cylindrical tube (sample holder) with an inner diameter of 7.2 mm and a cross-sectional area of $\sim 40\text{ mm}^2$ and

was put on the steel substrate. A load of 250 *g*, equivalent to a pressure of around 60 *kPa*, was applied to the oil sands on a homemade stage (pressure control unit). The pressure is larger than the maximum load experienced by the area on the truck with most carryback after dumping.

The X-ray source was operated at a voltage of 80 *kV* and a current of 126 μA for 5 to 6 hours per scan. The spatial resolution of the micro-CT scanning is 4.25 μm /pixel. With the high contrast in the obtained images, we were able to differentiate the compositions of oil sand samples into 3 parts: solids, liquids (bitumen and water), and air. The microstructure of solid/liquid/air phase and the volume fraction of those phases were analyzed using Dragonfly Pro software (Object Research Systems, Canada).

2.1.4 Quantitative measurements of frozen oil sand adhesion

To quantitatively evaluate the adhesion strength of ice to solid substrate, multiple measuring setups have been studied and applied in researches related with ice adhesion study. The most commonly adopted test methods in laboratory study of ice adhesion includes tensile test[71, 72], horizontal/vertical shear test[13, 23, 48, 73], and centrifuge test[74, 75]. For the work principle of the horizontal shear test, the fracture force of ice column with a known contact area under shearing pushing force can be precisely measured by a force transducer, and the adhesion strength can be easily collected from the force-displacement (or force-time) curve[76, 77]. Compared with the other methods, the shear test method has advantages of simple structure and high accuracy. Hence, the shear test method has been widely used in ice-adhesion related works[13, 45, 56, 78, 79].

The adhesion strength of oil sands on solid substrates was measured using a custom-built setup (Figure 2.1(a)), adapted from the methodologies for ice adhesion measurements in literature[16, 71]. A ceramic Peltier plate was used to control the temperature of the substrate. The heat produced on the opposite face of the Peltier plate was

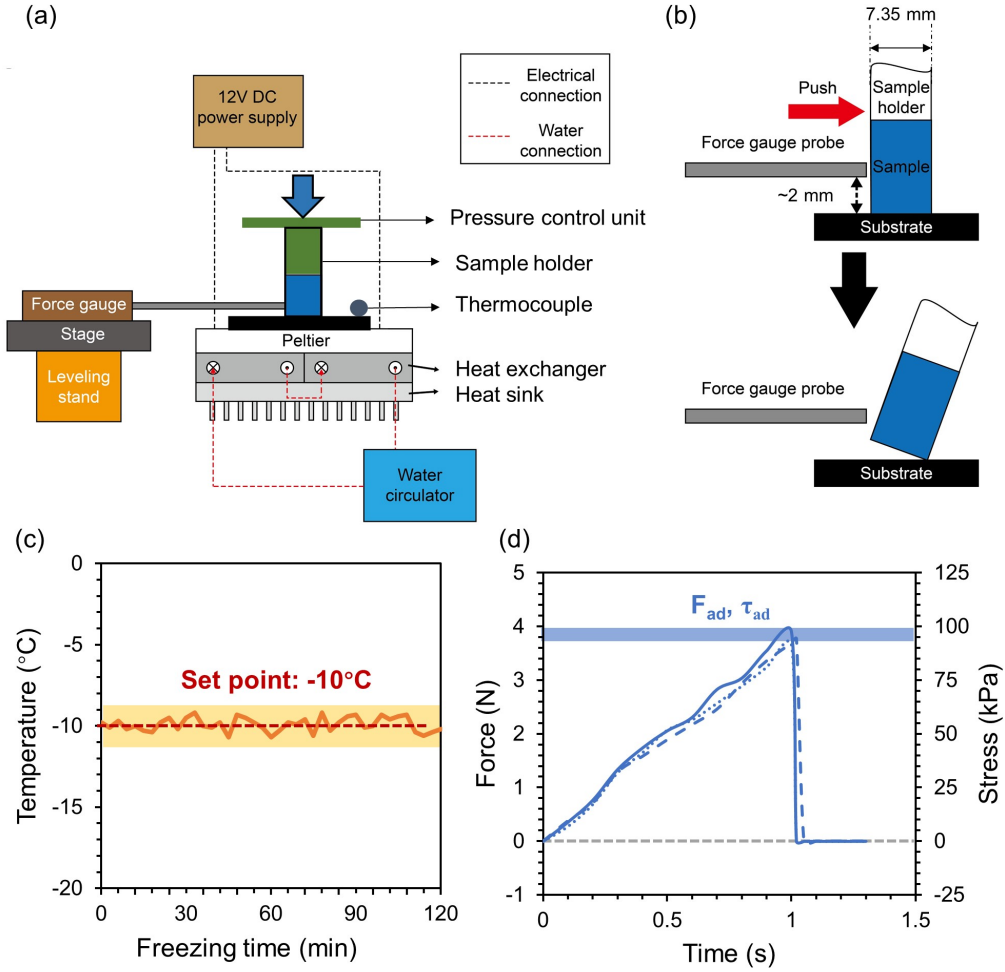


Figure 2.1: Adhesion strength measurement device and test procedure. (a) Schematic of the setup. (b) A force gauge measures the force applied to the frozen oil sand to the point of detachment. (c) Representative temperature curve on the Peltier stage around the set point temperature of -10°C (denoted as the red dashed line, with the variation indicated by the yellow band). (d) Force/stress curves during the ice adhesion strength measurements on PDMS substrate (3 repeats). The blue band shows the variation of the detaching force (F_{ad})/adhesion strength (τ_{ad}) of ice from PDMS substrate.

continuously removed by a water circulation system and a fin-type heat sink. The substrate was attached to the Peltier plate via thermally-conductive double sided tape, and a thermocouple was connected to the substrate to monitor the temperature.

About 0.3 g of oil sands was placed into the sample holder (same as the one used for CT scan). Then, a pressure of 60 kPa was applied on the sample with the pressure control unit (also the same as the one for CT scan). The load was kept on the

sample for a preset freezing time, beginning from the moment when the substrate reached the target temperature. During the freezing process, the temperature of the substrate remained within ± 1 °C of the set-point, as monitored by the thermocouple (Figure 2.1(c)). The load was removed before a force was applied to push the frozen sample.

Figure 2.1(b) shows the detaching process of the samples from the substrates. To apply a force parallel to the substrate, a force gauge probe attached to a linear motor was placed < 2 mm above the substrate. The short distance enabled minimal torque applied to the sample before detachment[71]. Figure 2.1(d) shows the force curves from three repeated measurements of ice adhesion strength on PDMS substrates after freezing water in the sample holder at -10 °C for 30 min. As the linear motor moves at a constant speed of 0.7 mm/s, the applied force increases linearly with time at 4 N/s until it reaches the minimal force required to detach the ice column at which point the force falls back to zero. The minimal detachment force F_{ad} for the three repeats are highly reproducible. The adhesion strength τ_{ad} obtained by normalizing the force by the contact area of 40 mm² was 95 ± 6 kPa, within the reported literature values of 70 to 100 kPa under similar experimental conditions [46–49, 65]. The good reproducibility of the adhesion strength suggests the reliability of our methodology.

2.2 Methods and procedure for Chapter 4

2.2.1 Preparation of substrates

Six types of substrates were used in this work. The substrates can be classified as hard and soft, based on the scale of Young’s modulus. The hard substrates include Silicone-epoxy-coated steel substrate (Silikopon EF, Evonik, Germany), chromium-carbide-overlay (CCO) (Imperial Oil, Canada), and steel 304 (McMaster-Carr, USA). The soft substrates are oil-resistant Buna-N nitrile rubber (McMaster-Carr, USA), poly(dimethylsiloxane) (PDMS) (Sylgard 184, Dow Corning, USA), and structured

PDMS. The fabrication of structured PDMS slab was described in another paper[80], and the procedure was provided in Supporting information.

For hard substrates, the steel substrate was cut into square-shaped plates with the dimensions of $4\text{ cm} \times 4\text{ cm}$. CCO was first cut into rectangular-shaped plates with the dimensions of $7\text{ cm} \times 5\text{ cm}$, and polished by a diamond grinding wheel (D150N100b1/8, USA) mounted on a surface grinder for 30 min . To fabricate the silicone-epoxy coated steel substrate, the elastomer base, Silikopon EF, was mixed rigorously with the curing agent, (3-Aminopropyl) triethoxysilane (APTES) ($>99\%$, Sigma, USA), by weight ratio of 4.5:1. After applying about 2 g of the mixed prepolymer to a cleaned steel substrate, the fully coated substrate was put under ambient temperature for over 24 hr to cure.

For soft substrates, oil-resistant Buna-N nitrile rubber were cut into the same shape of the steel plates, with the dimensions of $4\text{ cm} \times 4\text{ cm}$. To fabricate the PDMS substrate, a base and a curing agent were mixed rigorously at a weight ratio of 10:1. About 2 g of the mixed elastomer was cast onto a clean glass slide ($7\text{ cm} \times 2\text{ cm}$) to fully cover the slide surface with a thickness of about 1 mm . After degassing for 30 min and curing at the temperature of 80°C for 2 hours, the substrate coated with PDMS were placed under ambient conditions to cool down before use. The structured PDMS substrate was fabricated in a square shape with the dimensions of $6\text{ cm} \times 6\text{ cm}$. Before use, all the substrates were rinsed with acetone ($>99.5\%$, Fisher), ethanol ($>99\%$, Fisher), and deionized water. The reagents (acetone and ethanol) were used as received without additional treatment.

The contact angles of water on the substrates were determined by using a contact angle instrument (DSA100 system, Kruss, USA). The advancing and receding contact angles of water are shown in Table 2.3. The Young's modulus of the substrates were cited from literature, except for the rubber substrate, which was provided by the vendor (Macmaster-Carr).

To simulate the industrial environment where the substrate is often fouled by oil

Table 2.3: Contact angle of water and Young’s modulus of substrates

Substrate	θ_{adv} ($^{\circ}$)	θ_{rec} ($^{\circ}$)	Hysteresis ($^{\circ}$)	Young’s modulus
Stainless steel	92 \pm 2	21 \pm 4	71	\sim 200 <i>GPa</i> [81]
CCO	71 \pm 3	20 \pm 4	51	\sim 300 <i>GPa</i> [82]
Silikopon EF	100 \pm 3	69 \pm 4	31	\sim 3 <i>GPa</i> [83]
Rubber	109 \pm 3	58 \pm 3	51	3.2 <i>MPa</i>
Bare PDMS	121 \pm 3	47 \pm 4	74	1 <i>MPa</i> [84]
Structured PDMS	134 \pm 2	132 \pm 1	2	1 <i>MPa</i> [84]

sands stain, we also prepared steel substrates with an oil sands layer. To coat the steel substrate with oil sands, about 10 *g* of oil sands with C_w of 10 wt% was smeared uniformly on a piece of steel plate and pressed with a load of 0.06 *MPa* for close contacting. The fabrication of oil sands with C_w higher than 4 wt% was described in our previous work.[85] After removing the excess oil sands not touching the substrate, the coated substrate was placed in a freezer at a temperature of -10 $^{\circ}$ C for 1 *hr* to freeze. To avoid contamination and eliminate the variation in water content of the oil sands layer, the coated substrate was wrapped in a paraffin film before put in the freezer. The substrate was stored in the freezer until the experiment to prevent the oil sands from thawing and melting.

2.2.2 Spray coating and stability test of anti-freezing liquid

To mitigate the adhesion strength of wet granular matrix on solid substrates, we spray-coated the substrates with an anti-freezing liquid before applying the oil sands. Aqueous solutions of ethylene glycol (EG) (>98%, Sigma) and propylene glycol (PG) (85 v% with 15 v% of water, Sigma) were used as anti-freezing liquids. The solutions were diluted by water to reach a formulation of 2 or 3 parts of either EG or PG to 1 part of water by volume. The prepared anti-freezing liquid was stored in a spray bottle before use. For the test, certain amount of the anti-freezing liquid was sprayed

on the substrate to reach a uniform distribution of about 0.01 mL of liquid per cm^2 of the substrate.

To evaluate the stability of the anti-freezing liquid, we first sprayed $\sim 0.2 \text{ mL}$ of EG solution (EG:water = 2:1) on our steel substrate ($4 \text{ cm} \times 4 \text{ cm}$) and observed the profile of the sprayed droplets. With the side-view camera from the contact angle instrument, we observed and recorded the height and the base diameter of a droplet for over 3 hr under ambient conditions. We also observed the lateral profile of anti-freezing liquid under external forces to simulate the friction from wind after sprayed the liquid in real applications. To simulate the wind in the real scenario, we used a spin coater (WS-650Mz, Laurell, USA) to create a steady spinning speed of 500 revolutions-per-minute (RPM). After spraying $\sim 0.2 \text{ mL}$ of EG solution (EG:water = 2:1) on our substrates ($4 \text{ cm} \times 4 \text{ cm}$), the substrates were mounted to the spin coater and spun for 60 sec at 500 RPM. The profile of a droplet at the rim of the substrate, where the centrifugal force is at maximum on the substrate, was observed by the side-view camera before and after the spinning test. The adhesion strength of the anti-freezing liquid drop was calculated by dividing the centrifugal force with the contact area of the droplet.

2.2.3 Procedure for large scale tests

To test the feasibility of anti-freezing liquid spray for easy removal of frozen oil sands, we conducted the adhesion measurement of oil sands ($C_w = 4 \text{ wt}\%$) on a large stainless steel plate ($1.2 \text{ m} \times 0.6 \text{ m}$) sprayed with $\sim 100 \text{ mL}$ of EG solution (EG:water = 2:1). Subsequently, about 5 kg of oil sands were dumped on the steel substrate under ambient condition. The possible contact area between oil sands and the coated substrate was $530,000 \text{ mm}^2$. An additional load from a box of weight of around 53 kg was placed on the oil sands, creating a load of $\sim 0.01 \text{ MPa}$, as shown in Figure 2.2 (a). After loading, the substrate with oil sands was transferred into a walk-in freezer and kept at $-18 \text{ }^\circ\text{C}$ for over 2 hr . After freezing, the load was removed and the substrate

was held vertically to check if the oil sands can be removed by gradually adding a pushing force, as shown in Figure 2.2 (b). The pushing force was applied by gently placing a cardboard on the oil sands and adding a weight from the top to make the force parallel to the steel plate. The test was also performed with pristine, uncoated stainless steel substrate as control.

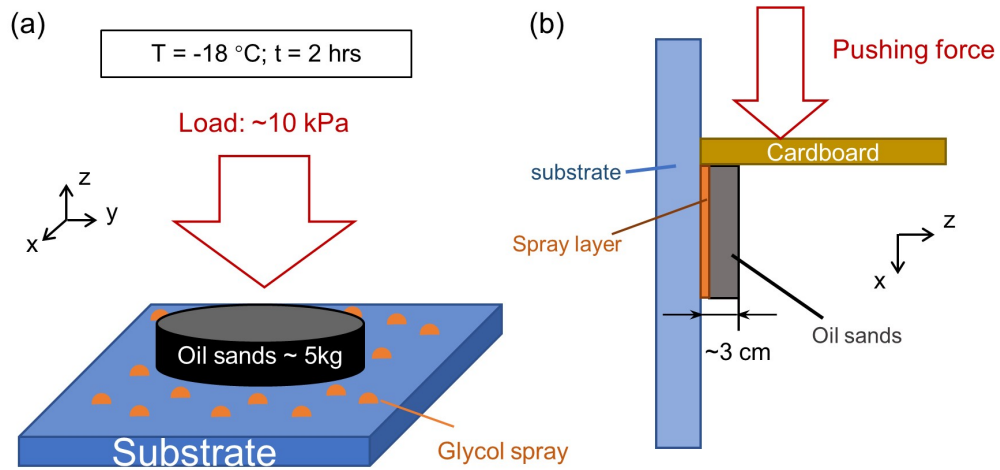


Figure 2.2: Schematic of large scale test procedure with the glycol spray. (a) - Process of oil sands sample freezing on the substrate sprayed with anti-freezing liquids under a load of ~ 0.01 MPa; (b) - Process of oil sands removal after frozen by adding weight on the cardboard.

Chapter 3

Water-mediated adhesion of oil sands on solid surfaces at low temperature¹

In chapter 3, we will show that the strong adhesion of oil sands at low temperature (0 °C to -20 °C) is determined by freezing of water in oil sands. With x-ray micro-computed tomography (micro-CT), between the sand particles and the solid substrate, we observed water capillary bridges, which contribute to adhesion strength when frozen. We identified a linear relationship between the adhesion strength and the water content in oil sands, based on the local contact area between ice and the solid surface. The insights from our study can help mitigate fouling from oil sands in winter. To the best of the authors' knowledge, this research work is the first study about the adhesion of a frozen granular matter to solid substrates, which may have wider applicability to many natural and industrial processes.

3.1 Oil sands microstructure

The microstructures of oil sands are characterized using X-ray micro-CT scanning. The images in Figure 3.1 (a) and (b) show the horizontal cross sections for $C_w = 4$ and 14 wt% close to the solid substrate $z < 0.01$ mm. At $C_w = 4$ wt%, we observed large

¹This section contains modified parts of submitted work **Q. Yang**, J. B. You, B. Tian, S. Sun, D. Daniel, Q. Liu, X. Zhang. Water-mediated adhesion of oil sands on solid surfaces at low temperature, Fuel. (2021)

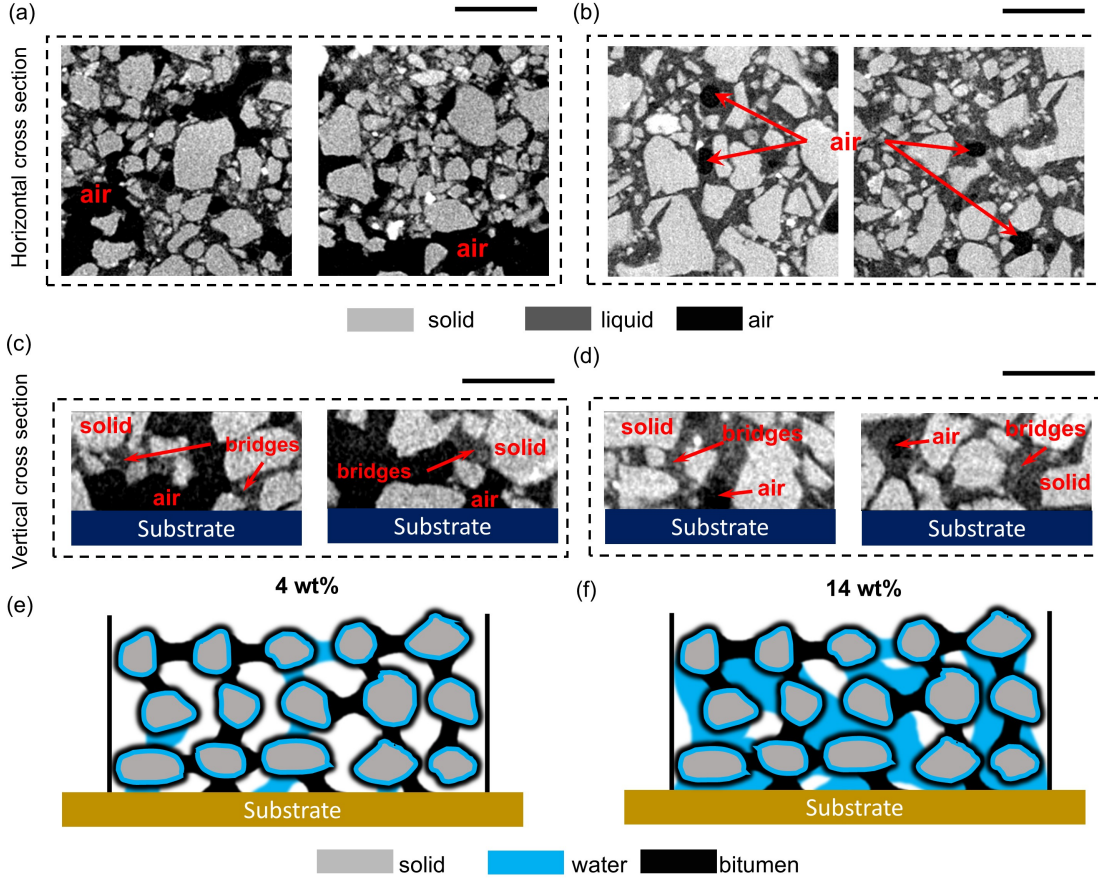


Figure 3.1: (a, b) Horizontal cross section of the oil sands with $C_w = 4$ and 14 wt% taken near the substrate $z \approx 0$ using a micro-CT. Scale bars are 0.5 mm. (c, d) The vertical cross section of the same oil sand with $C_w = 4$ and 14 wt%. The area was picked within the distance range from the substrate of near 0 to 0.25 mm. Scale bars are 0.25 mm. (e, f) Oil sand is a wet granular matter with solid sand particles held together by liquid (bitumen and water) capillary bridges. Increasing water content results in a more compact structure with fewer air gaps.

millimetric air gaps (Figure 3.1 (a)), whereas at $C_w = 14$ wt%, only submillimetric-sized air gaps remain (Figure 3.1 (b)). We were able to distinguish the solid, liquid and air phases, and their relative compositions are summarized in Table 3.1. Note that we are not able to distinguish between bitumen and water, because their densities are close to each other, both around 1.0 g/cm^3 [86].

Based on the micro-CT results, we propose the following model of oil sands microstructures after compression. The sand particles are polydisperse with sizes ranging from tens to hundreds of microns. At low water content $C_w = 4$ wt%, the sand

Table 3.1: Compositions of oil sand samples after compression at 60 *kPa*. z : the distance from the substrate.

C_w (wt%)	z (mm)	Volume fraction(%)		
		Solids	Liquids	Air
4	0–0.25	54.2	21.8	24.0
	0.25–0.50	54.9	18.9	26.2
14	0–0.25	56.3	34.5	9.2
	0.25–0.50	55.7	36.5	7.8

particles (about 55 v%) are held together mostly by bitumen capillary bridges (due to the low water content), with significant amount of air gaps (about 25 v%). A thin hydration layer also likely envelopes the sand particles, separating the hydrophilic silica surface and the hydrophobic bitumen [87], as depicted in the schematic in Figure 3.1 (e). Increasing the water content (from 4 to 14 wt%) results in a more compact structure with smaller air gaps as the water occupies some of the pore spaces (Figure 3.1 (f)), similar to the transition from the pendular to funicular state in wet granular matter [44]. Increasing C_w from 4 to 14 wt% reduces the volume of air gaps by a similar percentage from about 25 v% to less than 10 v%.

At higher $C_w = 14$ wt%, the sand particles are held together by a combination of water and bitumen capillary bridges (Figure 3.1 (f)); the bitumen bridges are not likely to be displaced because of the highly viscoelastic nature of bitumen at the temperature range in the experiments. Vertical cross sections also reveal the formation of water capillary bridges (which become ice at low temperatures) linking the sand particles and the solid substrate when increasing water content from $C_w = 4$ to 14 wt% (c.f. Figure 3.1 (c) and (d)).

At low temperatures, the adhesion between oil sand sample and a solid substrate comes from 4 material types: sand particles, air, ice, and bitumen. Among them, the interaction between air and the substrate is negligible, but that between ice and

the substrate is the strongest. This explains why increasing water content results in a dramatic increase in adhesion strength of frozen oil sands as will be discussed in the next section. Note that while oil sands typically contains 4 to 6 wt% water, water content can be much higher than 6 wt% during winter, when ice and snow is abundant at the mining site.

3.2 Oil sands adhesion in the limit of short freezing time

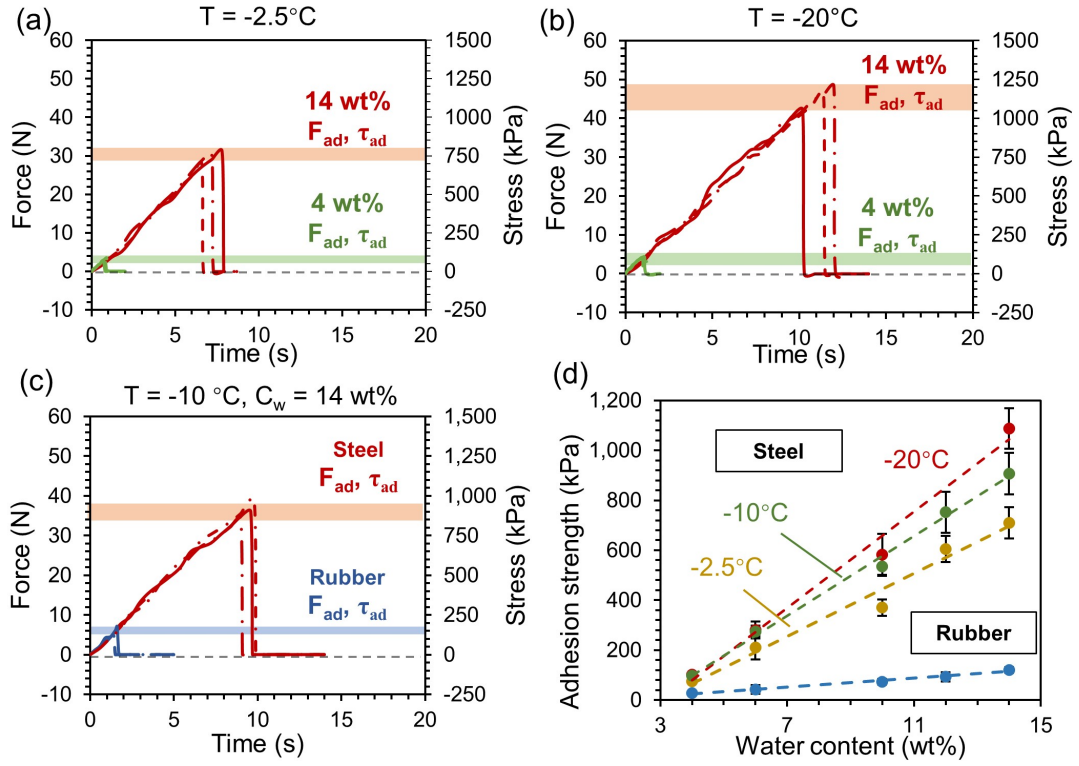


Figure 3.2: τ_{ad} of oil sands with $C_w = 4$ –14 wt% on steel substrate after 5 min of freezing. (a, b) Representative force curves at $T = -2.5$ °C and -20 °C on steel substrate, respectively, with 3 repeats for each C_w value. (c) Representative force curves at $T = -10$ °C on rubber and steel substrates. (d) Plot of τ_{ad} as a function of C_w on steel and rubber substrates. Error bars in (d) are standard deviations for 5 repeats.

We measured the oil sand adhesion to pristine steel surfaces τ_{ad} (obtained by dividing the adhesion force F_{ad} and the contact area of 40 mm^2) for $C_w = 4$ to 14 wt% in the limit of short freezing time $t = 5 \text{ min}$. Figures 3.2 (a) and (b) show the force

curves for $C_w = 4$ and 14 wt% obtained at $T = -2.5$ °C and -20 °C, respectively. Note that above the freezing point of water, i.e. $T > 0$ °C, τ_{ad} is not measurable (below the instrument limit of 2 kPa) regardless of water content C_w .

As C_w increased from 4 to 14 wt%, τ_{ad} increased by almost 10 times from 74 ± 7 kPa to 710 ± 60 kPa at $T = -2.5$ °C (Figure 3.2 (a)). The same ten-fold increase in τ_{ad} (from 107 ± 12 kPa to $1,090 \pm 90$ kPa) was also observed at $T = -20$ °C (Figure 3.2 (b)). At a given temperature, the adhesion strength increases with water content C_w (Figure 3.2 (d)), consistent with our hypothesis that ice formation at the sample-substrate interface is key to understanding the strength of oil sands adhesion at low temperatures. The approximate linear relationship between τ_{ad} and C_w may be rationalized by the increase in the contact area of ice and the substrate surface A_{ice} . As discussed in the previous section, there are water capillary bridges connecting the oil sand and the surface, which can freeze when $T < 0$ °C. The contact area of water capillary bridges A_{water} (and hence of ice contact area A_{ice} after freezing) should increase linearly with C_w . Hence, we expect F_{ad} and τ_{ad} to increase linearly with C_w , as we observed experimentally in Figure 3.2 (d).

Note that even at the highest water content level ($C_w = 14\%$) and lowest temperature tested ($T = -20$ °C), the measured $\tau_{ad} \approx 1,100$ kPa is still lower than the $\tau_{ad} = 1,250$ kPa previously reported for pure ice on steel [78, 79], reflecting the fact that surface ice coverage in oil sands is only partial. We tried to measure the adhesion strength of pure ice on steel with our setup. But the adhesion strength of ice on steel exceeded the upper limit of our force apparatus of 1,200 kPa . Hence, we quoted the value of ice adhesion strength on steel from the literature.

Interestingly, also shown in Figure 3.2 (d), τ_{ad} increased almost linearly from 24 ± 9 kPa to 125 ± 30 kPa with C_w from 4 to 14 wt% on a rubber substrate at -10 °C for 5 min of freezing time. This result confirms that water content in oil sands is also essential for the rubber substrate, and the model which we proposed in Figure 3.1 is not limited to steel. Compared with τ_{ad} on steel substrate under same conditions,

τ_{ad} on rubber substrate was about 15-20% of the value for oil sands with the given C_w level. The softness and hydrophobicity of the substrate may decrease τ_{ad} on the rubber, based on the influence of substrate properties on ice adhesion strength[46–49, 65].

τ_{ad} is higher at lower temperature at a given C_w level, suggesting that the short freezing time $t = 5 \text{ min}$ may not be long enough for water to freeze completely. In other words, the measured τ_{ad} values in Figure 3.2 may not be the equilibrium values and therefore depend on the ice nucleation rate. From classical nucleation theory, the ice nucleation rate (J) is given by the Arrhenius equation[88]

$$J = A \cdot \exp\left(-\frac{\Delta G}{K_B T}\right) \quad (3.1)$$

where A is the pre-exponential factor, K_B is the Boltzmann's constant, T (in Kelvin) is the absolute temperature. The activation energy ΔG is given by[88]

$$\begin{aligned} \Delta G &= \frac{16\pi}{3} \frac{\gamma^3}{\Delta S^2 \Delta T^2} f(\theta) \\ &= \frac{16\pi}{3} \frac{\gamma^3 T_m^2}{L_v^2 \Delta T^2} f(\theta) \end{aligned} \quad (3.2)$$

γ ($\approx 20 \text{ mN m}^{-1}$) is the water-ice interfacial energy, ΔS ($= L_v/T_m$) is the entropy of fusion, with L_v of $3.34 \times 10^8 \text{ J m}^{-3}$ (the specific latent heat of fusion for ice) and T_m of 273.15 K (the melting point for ice), and ΔT ($= T - T_m$) is the degree of supercooling. $f(\theta)$ is a geometrical factor that depends on the contact angle of water on steel.[89]

$$f(\theta) = \frac{(2 + \cos \theta)(1 - \cos \theta)^2}{4} \approx 3 \times 10^{-3} \quad (3.3)$$

From the measured receding contact angel of water on steel substrate, which is approximately 20° , we estimated $f(\theta)$ to be 3×10^{-3} in our experiments. Thus, Eq.(3.1) and (3.2) can be rearranged to

$$\begin{aligned}
J &= A \cdot \exp\left(-\frac{C}{\Delta T^2}\right) \\
C &= \frac{16\pi}{3} \frac{\gamma^3 T_m^2}{L_v^2 K_B T} f(\theta) \\
&\approx \frac{16\pi}{3} \frac{\gamma^3 T_m}{L_v^2 K_B} f(\theta) = 71 K^2
\end{aligned} \tag{3.4}$$

The ice nucleation rate (J) is therefore highly dependent on ΔT , with a constant $C \approx 71 K^2$ that depends on the material properties of water and the substrate.

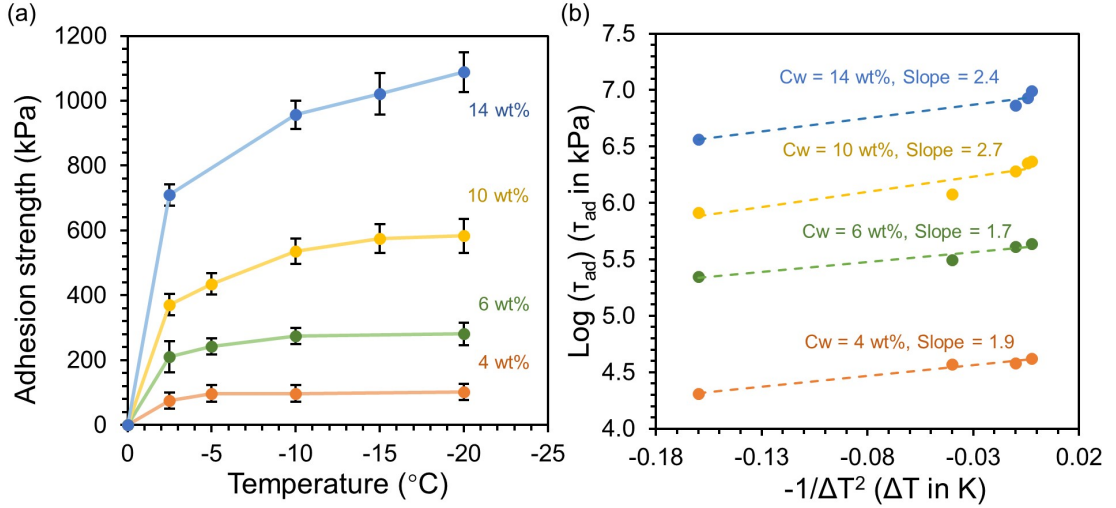


Figure 3.3: (a) τ_{ad} of oil sand samples with different C_w to steel as a function of T after 5 min of freezing time. At $T = 0$ °C, τ_{ad} is too low to be measured for all C_w levels. Lines are guides to the eye. Error bars are standard deviations for 3 to 5 repeats. (b) Plot of $\log(\tau_{ad})$ against $1/\Delta T^2$ for the same data in (a). τ_{ad} and ΔT have units of kPa and K, respectively.

To verify that $\tau_{ad} \propto A_{ice} \propto J$, we varied T from -2.5 to -20 °C and measured τ_{ad} while keeping the freezing time constant at 5 *min*. Indeed, τ_{ad} increases with increasing ΔT for all C_w values (Figure 3.3.(a)). Plotting $\log \tau_{ad}$ against $-1/\Delta T^2$ also results in straight lines with slopes ranging from 1.7 to 2.7 K². The linear trend and the similar slopes are just as predicted by Equation 3.4 (Figure 3.3.(b)). In the limit of short freezing time, the adhesion strength is therefore limited by the ice nucleation rate and hence the degree of supercooling ΔT . In contrast, with longer freezing time, the adhesion strength approaches the equilibrium value and no longer depends on ΔT , as will be discussed in the next section.

3.3 Oil sands adhesion in the limit of long freezing time

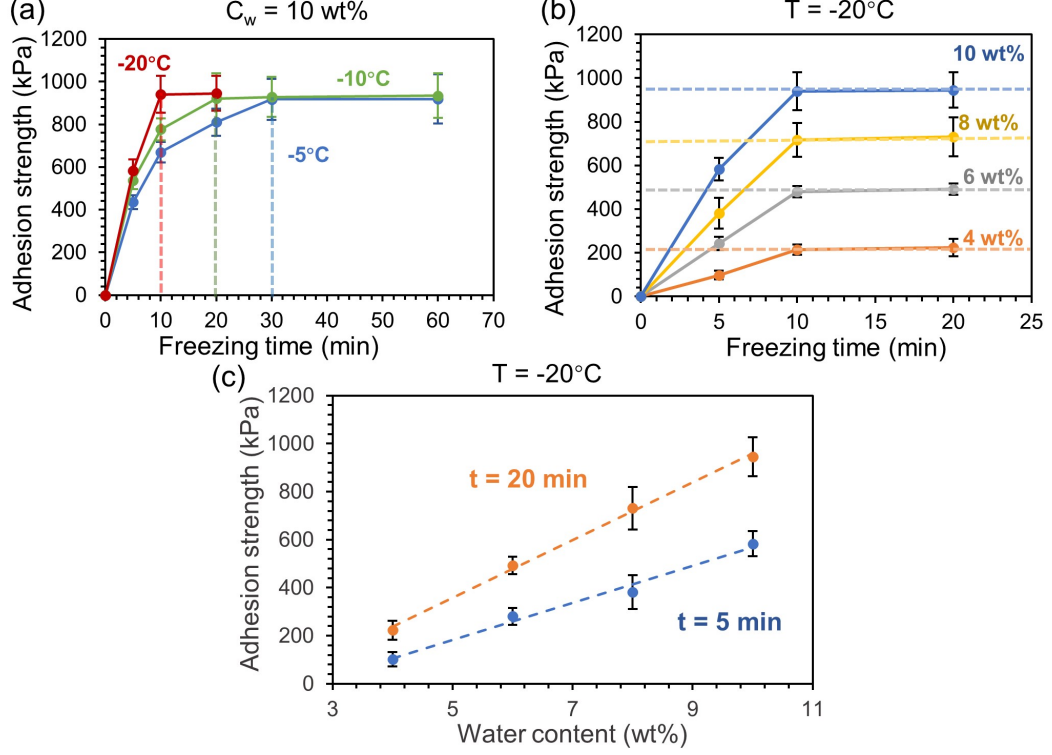


Figure 3.4: Equilibrium τ_{ad} after longer freezing time. (a) - Results of oil sands τ_{ad} with longer freezing time for oil sands with C_w 10 wt% at -5°C to -20°C . Each color of the line denotes the results at a certain temperature. The dashed lines with corresponding color denotes the plateau time; (b) - τ_{ad} for oil sands with C_w of 4 to 10 wt% at -20°C with 5 to 20 min of freezing time. Each color of the lines denotes a certain C_w level. The dashed lines of corresponding color label out the plateau for a C_w level; (c) - Results of linear fitting for τ_{ad} and C_w at -20°C with 5 and 20 min of freezing time. Error bars show the standard deviation from 3 to 5 repeated tests.

To obtain the equilibrium τ_{ad} values, we increased the freezing time from 5 to a maximum of 60 min. Figure 3.4 (a) shows that after sufficient freezing time, most (if not all) of the water is frozen and τ_{ad} for $C_w = 10 \text{ wt}\%$ reached a plateau or its equilibrium value of approximately 950 kPa . τ_{ad} is not limited by the ice nucleation rate and is therefore independent of $T = -5^\circ\text{C}$, -10°C , and -20°C . The time taken for τ_{ad} to plateau $t_{plateau} \sim 10 \text{ min}$ was the shortest at the lowest temperature of $T = -20^\circ\text{C}$, which doubled to $\sim 20 \text{ min}$ at $T = -10^\circ\text{C}$, and tripled to $\sim 30 \text{ min}$ at $T = -5^\circ\text{C}$.

Table 3.2: Conditions and results of τ_{ad} ($C_w = 10$ wt%) measurement with EG spray measured after 5 *min* of freezing. The standard deviation was from at least 3 repeated tests.

Substrate	Temperature (°C)	τ_{ad}	τ_{ad} after spray
Steel	-5	435 ± 33 <i>kPa</i>	
Steel	-10		< 2 <i>kPa</i>
Steel	-20		
Bitumen-coated	-5	998 ± 103 <i>kPa</i>	
Bitumen-coated	-10		< 2 <i>kPa</i>
Bitumen-coated	-20		
Asphaltene-coated	-5	611 ± 66 <i>kPa</i>	< 2 <i>kPa</i>

Figure 3.4 (b) shows that the plateau adhesion strength increases with water content in oil sands, and importantly $t_{plateau} \sim 10$ *min* is independent of $C_w = 4$ to 10 wt%. Interestingly, τ_{ad} is linearly proportional to C_w both for long freezing $t = 20$ *min* (when τ_{ad} reaches its plateau value) and short freezing $t = 5$ *min* (when τ_{ad} is limited by ice nucleation rates), as shown in Figure 3.4 (c).

3.4 Mitigation of oil sands adhesion on multiple substrates

To mimic the situation of pre-fouled substrates in the industry, we measured τ_{ad} on bitumen and asphaltene coated substrates. For oil sands with 10 wt% of water at -5 °C for 5 *min* of freezing time, the results in Table 3.2 show that τ_{ad} was higher on the coated substrates ($\sim 1,000$ *kPa* on bitumen-coated and ~ 600 *kPa* on asphaltene-coated). Lower adhesion on the steel substrate may be attributed to its high roughness, as suggested by the large hysteresis of water on the substrate (Table 2.1) and the optical images. Reduced number of capillary bridges formed between oil sands and the rough steel substrate.

Since the adhesion strength of oil sands to solid substrates are dominated by ice

formation at low temperatures, an effective strategy to mitigate oil sands adhesion is to prevent ice formation in the first place. To this end, before placing the oil sands, we spray the steel surface with a commonly used anti-freezing liquid ethylene glycol (EG, >99.8%, Sigma) which is known to depress the freezing temperature of water T_m . For example, a mixture of 60 v% EG and 40 v% water freezes at -45 °C. We found that pre-spraying both pristine and bitumen-coated steel surfaces with EG reduces τ_{ad} to a value lower than the detectable limit of our set up ($< 2 \text{ kPa}$) not only for $T = -5 \text{ °C}$, but even for -20 °C. The reduction in τ_{ad} was significant compared with the data shown in Table 3.2. Table 3.2 summarizes the experimental conditions that we have tested; for each test, we performed at least 3 repeats. Note that the ultra-low adhesion strength observed ($< 2 \text{ kPa}$) is at least as good as the best-performing anti-icing surfaces. Details of the EG spray formulation will be reported in a future publication.

3.5 Conclusions

In this Chapter, we found that water content is critical for the adhesion of oil sands (a complex granular matter) at low temperature. The images from our micro-CT measurements show that the air pockets in oil sands were filled with interstitial water, which forms capillary bridges with the substrate. The adhesion strength of oil sands increased linearly on steel and rubber substrate with increase in the water content, and also with the degree of supercooling within a short freezing time. Formation and adhesion of ice was shown to increase the adhesion strength of oil sands. Fouling from bitumen or asphaltene layer on the surface aggravates the adhesion of oil sands on steel. Based on the significant impact from ice in the granular matrix, we developed an effective approach to reducing the adhesion of oil sands by spraying an anti-freezing liquid on the substrate. No adhesion was detected after spraying.

Chapter 4

Effects of load and substrate properties on ice-enhanced adhesion of frozen oil sands¹

From chapter 3, we concluded that the adhesion strength of oil sands to solid substrates at low temperature was strongly correlated with the water contents in the granular matrix. With the help of X-ray computed tomography imaging system, we observed that interstitial water forms capillary bridges between the solid particles and the substrate, and the surface coverage of water bridges is the main contribution to the adhesion strength after frozen into ice.

So far, the effects from substrate properties and from the load sustained by the oil sands on the adhesion strength on solid substrates remain unclear. For natural oil sands, a certain amount of porosity exists within the matrix with voids not occupied by either bitumen or water.[90–92] The porosity of oil sands matrix influences the mechanical properties and behaviours of the oil sands, for example, under the shearing stress[93]. The volume of the void space depends on the water contents, which can reach 25 v% for oil sands with 4 wt% of water under 0.06 *MPa* of load [85]. With increasing load, the void spaces in the matrix may be replaced with the solid/liquid components.[92, 94]

¹This section contains modified parts of manuscript under preparation by **Q. Yang**, N. Moradpour, J. B. You, B. Tian, S. Sun, D. Daniel, Q. Liu, D. Wang, X. Deng, X. Zhang. Effects of load and substrate properties on ice-enhanced adhesion of frozen oil sands.

In chapter 4, we will show that the adhesion of oil sands resembles the adhesion behavior of ice on the same kind of substrates, including hard substrates with Young's modulus on the order of GPa and soft substrates with high deformability (Young's modulus on the order of MPa). On a hard substrate of steel, we found a correlation between the load on the sample and the adhesion strength of frozen oil sands, which was attributed to the packing mode of the sand particles. The anti-freezing liquids showed high potential to reduce the adhesion strength of oil sands on steel and oil sands-fouled substrates. The strategy is also applicable at a large scale (around 500 cm^2), which is greatly promising for real application in the oil industry.

4.1 Effects of surface properties on adhesion

τ_{os} and τ_{ice} on six substrates (shown in Table 2.3) was compared in our experiment. Among them, hard CCO is the most hydrophilic substrate (lowest advancing contact angle of $\sim 70^\circ$), and soft structured PDMS is the most hydrophobic with the highest advancing contact angle of $\sim 134^\circ$ and an ultra low contact angle hysteresis of only 2° . The influence of contact angle on ice adhesion strength strength on hard and soft substrates is shown in Figure 4.1.(a). Structured PDMS yielded the lowest ice adhesion strength ($\tau_{ice} = 39\text{ kPa}$). On the other hand, τ_{ice} on CCO was dramatically higher, 817 kPa . τ_{ice} on steel is too high to be measured within the detectable range of the force gauge in our apparatus. From the literature, τ_{ice} on steel is $\sim 1,250\text{ kPa}$ [78, 79].

Theoretical description of the relationship between ice adhesion strength and static water contact angle has been reported in the literature [95]. Thermodynamic work of adhesion of water on the substrate is expressed as below.

$$\tau = C_0(1 + \cos \theta_{rec}) \quad (4.1)$$

Where τ is ice adhesion strength in kPa , C_0 is a constant also in kPa related with

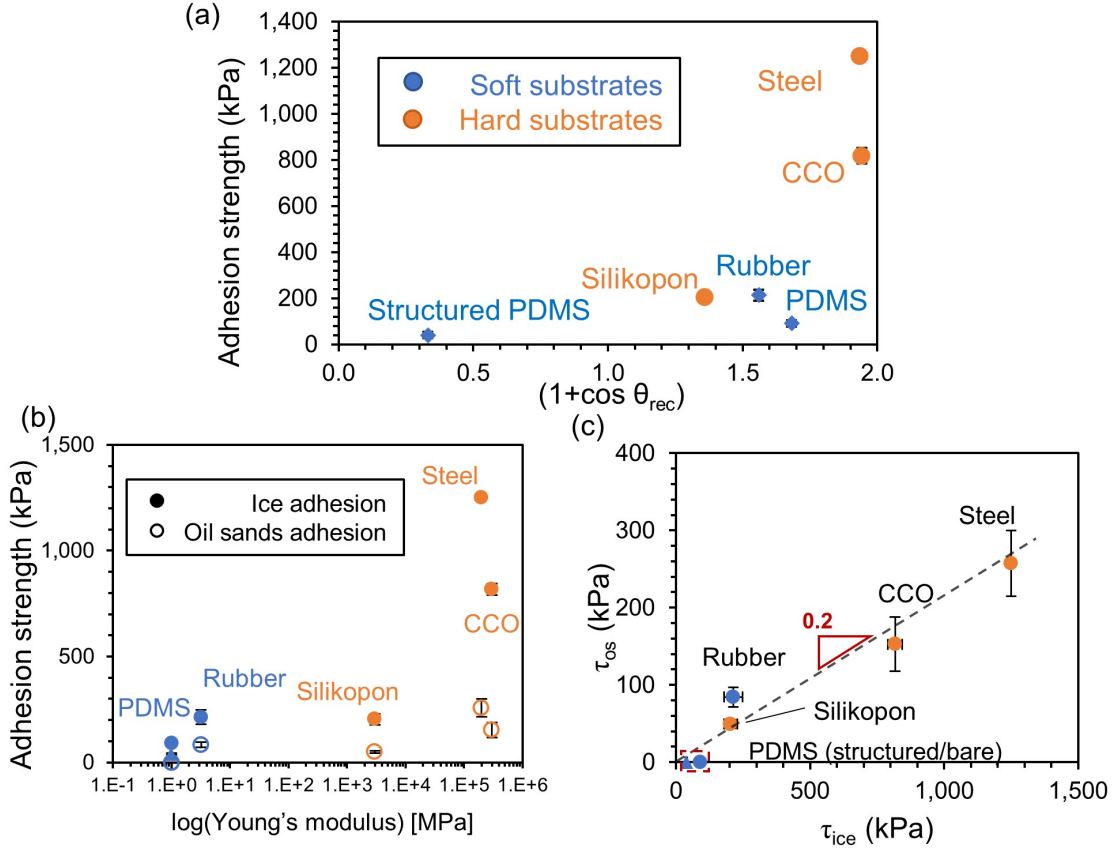


Figure 4.1: Effect of substrate surface properties on ice/oil sands adhesion strength on hard (Silikopon, CCO, and steel) and soft substrates (rubber, PDMS, and structured PDMS). (a) - τ_{ice} to work of detachment of water ($1 + \cos \theta_{rec}$) on hard (orange) and soft substrates (blue); (b) - τ_{os} and ice on both soft and hard substrates with the Young's modulus of the substrates in MPa . The oil sands were under $0.03 MPa$ of load before frozen; (c) - Linear relationship between τ_{os} and τ_{ice} on 6 substrates. τ_{os} on PDMS substrates (structured and bare) is below the minimum detectable range of our setup ($\sim 2 kPa$), labeled as $0 kPa$ on the plots. Error bars are standard deviation of at least 3 repeated measurements.

the surface tension of water, and θ_{rec} is the receding contact angle of water on the substrate representing the surface energy of the substrate. According to Eq.4.1, the relation between adhesion strength and $\cos \theta_{rec}$ was expected to be linear, which was not observed in Figure 4.1 (a). For hard substrates, ice adhesion could be enhanced by the surface roughness of the substrates[20, 22, 96], which increased the contact area between ice and substrate. This may explain the reason for the high τ_{ice} measured on CCO. Substrate deformability also influences the adhesion strength. The Young's modulus of ice is known to be on the order of 8 to 10 GPa [97, 98], which is at least

1,000 times higher than that of PDMS ($\sim 1 \text{ MPa}$) and rubber substrates ($\sim 3.2 \text{ MPa}$). Mismatched moduli of ice and soft substrates can cause stress concentration at the interface and facilitate ice detachment under shearing stress, and facilitate ice sliding on the soft substrate.[48, 80] The lower τ_{ice} on structured PDMS may be related to the Cassie-Baxter state of water at the interface, which provides less ice-solid contact area compared to rubber and flat PDMS substrate.

Importantly, on both hard and soft substrates, we demonstrated a clear correlation between τ_{os} and τ_{ice} . As shown in Figure 4.1.(b), both τ_{ice} and τ_{os} increased with the Young’s modulus of the substrate. Interestingly, τ_{os} on bare and structured PDMS surface were even below the minimum detectable range of our setup ($< 2 \text{ kPa}$), in agreement with the low τ_{ice} on PDMS substrate ($< 100 \text{ kPa}$). Results in Figure 4.1.(b) suggested that, for structured PDMS, the composition in the oil sand matrix may not penetrate into the microstructure. Otherwise, the effect of mechanical interlock would have increased τ_{os} on structured PDMS. Thus, the low τ_{os} on structured PDMS substrate is an indicator that water stayed in a ‘Cassie-Baxter’ state under 0.03 MPa of load.

Figure 4.1.(c) showed that the adhesion strength of oil sands τ_{os} increased with the ice adhesion τ_{ice} on both soft and hard substrates. In our recent work, we demonstrated the critical role of ice formation in the adhesion strength of a wet granular matter (oil sands) at low temperature. Freezing of water bridges formed between water in oil sands and the substrate led to strong adhesion of frozen oil sands[85]. The close correlation between τ_{os} and τ_{ice} in Figure 4.1.(c) further confirms that the ice formation on the solid surface is the primary reason for the adhesion strength of frozen oil sands.

The slope of the linear fitting in Figure 4.1.(c) was 0.2, suggesting that the surface coverage of ice on all six substrates was around 20%. Considering the weight percentage of each component in oil sands (4 wt% of water, 13 wt% of bitumen and 83 wt% of solids) and the density of each component (1 g/cm^3 for water and bitumen

and 2.4 g/cm^3 for sands), the maximal volume fraction of water was $\sim 10 \text{ v\%}$ in oil sands assuming no void space was present. The maximal surface coverage of water on the substrates was estimated to be $(10 \text{ v\%})^{2/3} \approx 0.22$, which is in good agreement with the slope of the linear fitting.

4.2 Effects of load on oil sands adhesion strength

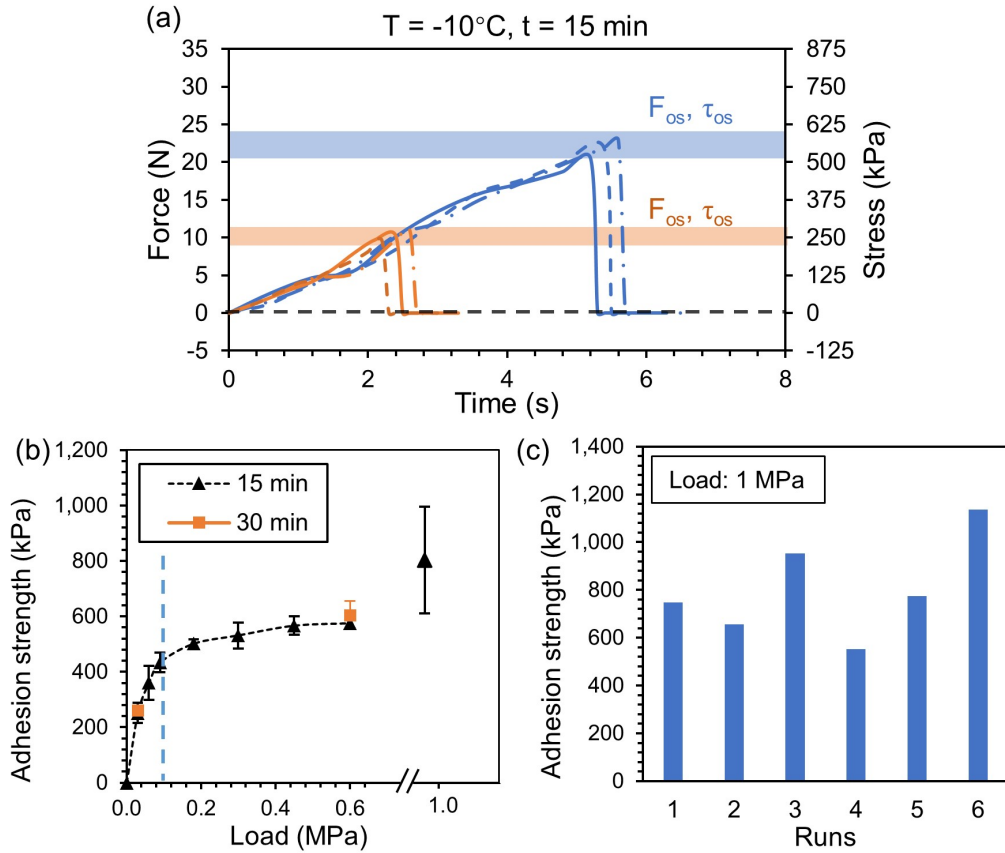


Figure 4.2: Effect of load on the τ_{os} . (a) - Representative force/stress curves for τ_{os} at $-10 \text{ }^\circ\text{C}$ for 15 min of freezing. The black dashed line denotes 0 N or 0 kPa of adhesion. Curves with orange/blue color are for oil sands under $0.03/0.6 \text{ MPa}$ of load. The colored box with corresponding color denote the minimum detaching force (F_{ad})/adhesion strength (τ) for frozen oil sands under 0.03 (orange) and 0.6 (blue) MPa of load. The height of the box denotes the variation of 3 repeated tests; (b) - Effect of load from 0 to 1 MPa on τ_{os} with a freezing time of 15 min and 30 min . The dotted line is at 0.1 MPa . Error bars are standard deviation of at least 3 repeated measurements; (c) - τ_{os} under an extremely high load of 1 MPa with 15 min of freezing time for 6 runs.

Figure 4.2.(a) showed the representative plots of force/stress versus time under

the load of 0.03 *MPa* (shown in color orange) and 0.6 *MPa* (shown in color blue). The slopes of the curves for all samples were similar to each other, indicating that the pushing velocity from the movable stage was steady. The colored boxes in Figure 4.2.(a) represented the range of variation in the adhesion force (F_{os})/strength (τ_{os}) for the samples. As shown, the boxes were narrow enough showing that both F_{os} and τ_{os} for all tested samples were measured with acceptable variation. After oil sands were detached from the substrate, we observed no residual sample left on the substrate, showing the rationality of normalizing by the apparent contact area between oil sands and the substrate.

In Figure 4.2.(b), we showed how τ_{os} varied with load applied on the oil sands samples for two different freezing times. With 15 *min* of freezing time, τ_{os} for oil sands rapidly increased from 0 to 450 *kPa* with the load on the sample from 0 to 0.1 *MPa*. Above applied load of 0.45 *MPa* up until 0.6 *MPa*, τ_{os} remained nearly plateaued at 550 *kPa*. The trend of τ_{os} increasing with the load and eventually reached a plateau. Adhesion strength was also measured for 30 *min* of freezing time (shown as orange points in Figure 4.2.(b)). Under the same load, no apparent difference was observed between τ_{os} obtained at 15 *min* and at 30 *min* of freezing time. Therefore, it is reasonable to assume that the equilibrium freezing time is \leq 15 *min* in our systems. The effect of the load on the adhesion strength of oil sands proved that our argument – water contact area dominates τ_{os} , is correct for oil sands adhesion to the steel substrate.

The increase in τ_{os} with the load from 0.03 to 0.1 *MPa* could be attributed to displacement of voids and some initial easy rearrangement of composition in oil sands. The previous work showed that after compression under 0.06 *MPa* of load, oil sands consisted of 55 v% of solids, 20 v% of liquids and 25 v% of air [85]. Under the load, the contact area initially occupied by voids (air) in loose oil sands could be replaced by liquids or solid particles. Moreover, water could transfer from the sample above to the substrate through stronger capillary effects in small gaps under the

compression[94]. Water accumulated at the substrate could form more bridges and larger contact area with the substrates, leading to the sharp increase in τ_{os} . As the load reached around 400 *kPa* and above, τ_{os} only increased slowly because of less mobility and deformability of the densely packed materials in oil sands.

However, at an even higher load of 1 *MPa*, the average value of τ_{os} increased significantly to ~ 800 *kPa*. We assume that peeling off of the bitumen layer under a high load may lead to an increase in the contact between water and the substrate surface. It was shown in the literature that the ultrasound and CO₂ pressure could enhance the bitumen liberation during the extraction process.[99, 100] The liberated bitumen may spatially rearrange, and the composition in the oil sands matrix may pack more densely, and thus, lead to higher adhesion strength. The large variation in τ_{os} under 1 *MPa* of load (Figure 4.2.(b)) may be attributed to random redistribution of the granular structure in each test.

4.3 Mitigation of adhesion by anti-freezing liquid

Spraying a layer of anti-freezing liquid, e.g. ethylene glycol, is an effective approach of reducing the adhesion strength of oil sands.[85] Here, to explore the applicability of anti-freezing liquids, we tested aqueous solutions of ethylene glycol and propylene glycol, which in principle could reduce the freezing point of water down to -40 °C. [101, 102] The solutions were spray coated on target substrates prior to testing them for the adhesion of frozen oil sands. Figure 4.3 shows the adhesion strength of the frozen oil sands sample on the substrates coated/uncotaed by one type of anti-freezing solution – EG:water = 2:1.

In Figure 4.3, apart from pristine steel substrates ($\tau_{os} \approx 250$ *kPa*), we also measured τ_{os} on the pre-fouled oil sands layer. The adhesion strength of oil sands with C_w of 4 wt% was over 700 *kPa*, which was around three times as high as the adhesion strength of oil sands to the bare steel substrate under the same conditions, demonstrating a stronger adhesion strength of oil sands to the fouled substrate. However, with the

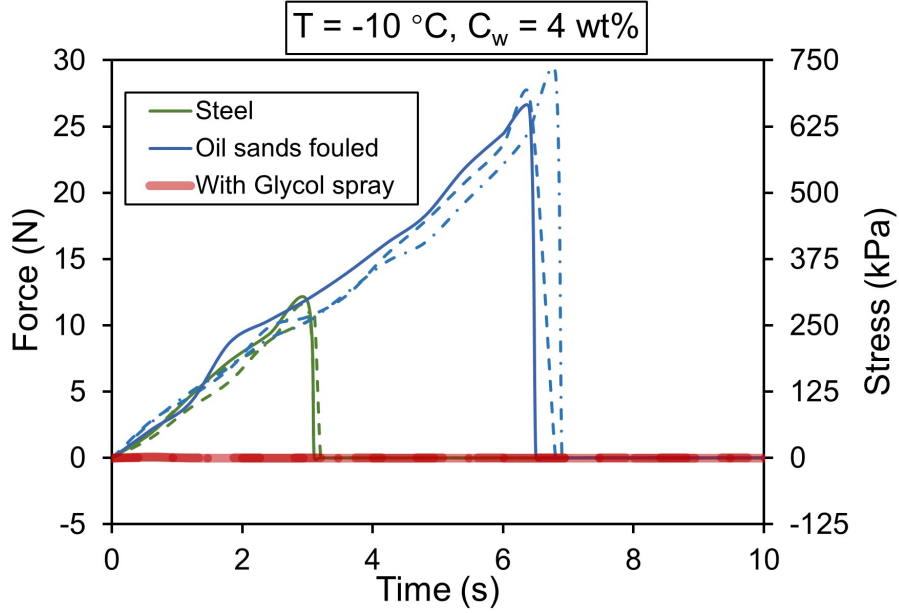


Figure 4.3: Representative force curves for oil sands adhesion strength on steel/oil sands fouled layer with/without glycol spray (EG:water = 2:1). Adhesion tests were performed with frozen oil sands with natural water concentration of 4 wt% under 60 kPa of load. The freezing temperature and time were -10 °C and over 2 hr.

outstanding performance of spraying a layer of glycol solution, τ_{os} on both pristine and fouled substrates reduced to almost undetectable at -10°C. Table 4.1 lists the condition and the adhesion strength of the frozen samples on the substrates coated by the anti-freezing solutions with different compositions. As shown by the table, the τ_{os} on the all of the spray coated substrates were lower than the detection limit of our apparatus, which was around 2 kPa.

From the data listed in Table 4.1, we could see that by spraying anti-freezing liquids with multiple compositions, τ_{os} decreased to almost undetectable not only on pristine steel substrate, but the oil sands-fouled substrates, which naturally has higher τ_{os} . In the oil industry, the surfaces are commonly pre-fouled by oil sands. In this case, the possibility for the spray to reduce the adhesion strength between oil sands and the pre-fouling layer endows it a broader application for anti-fouling purpose in the industry.

As shown in Figure 4.4.(a), we chose 2 characteristic parameters of a single droplet,

Table 4.1: Conditions and results of τ_{os} measurement with anti-freezing liquid spray.

Substrate	Anti-freezing liquid (v/v)	τ_{os}
Steel	Without spray	$\sim 250 \text{ kPa}$
Steel	EG:water = 3:1	$< 2 \text{ kPa}$
Steel	EG:water = 2:1	$< 2 \text{ kPa}$
Steel	PG:water = 3:1	$< 2 \text{ kPa}$
Steel	PG:water = 2:1	$< 2 \text{ kPa}$
Oil sands-fouled	Without spray	$\sim 700 \text{ kPa}$
Oil sands-fouled	EG:water = 2:1	$< 2 \text{ kPa}$
Oil sands-fouled	PG:water = 2:1	$< 2 \text{ kPa}$

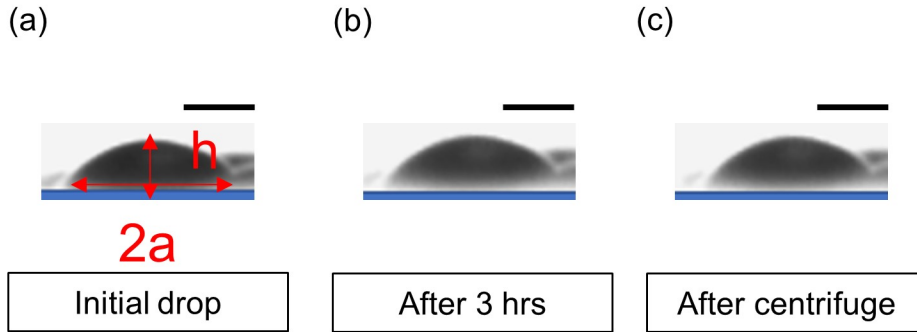


Figure 4.4: Volume change and lateral-view images of EG spray (EG:water = 2:1) droplets on steel substrate put under ambient conditions for 3 *hr* and after centrifuge. The black contrast denotes the presence of EG droplets. The droplet volume was calculated by assuming spherical cap shape. Characteristic parameters: a - base radius, h - height of the droplet. Length of scale bar: 0.1 *mm*;

namely the peak height (h) and base diameter (a), to determined the mass loss of the EG droplets for 3 *hr* under ambient conditions. The figure shows an EG droplet with $a = 0.25 \text{ mm}$ and $h = 0.14 \text{ mm}$. As shown by the plot in Figure 4.4.(b), the droplet remained unchanged even after 3 *hr*. Also, other droplets on the wafer showed no noticeable change in size after 3 *hr*. Thus, the sprayed EG droplets remained stable under ambient condition and the influence from evaporation was negligible.

Furthermore, to simulate the wind conditions in the environment, the spray coated

EG droplets were spun using a spin coater. The drop volume was around 15 mm^3 for the same droplet that we observed for 3 *hr*. After spinning, the EG droplet showed no noticeable change in the shape ($a = 0.25 \text{ mm}$, $h = 0.14 \text{ mm}$). The position of the droplet also remained the same after the spinning process, demonstrating a strong interaction of EG droplet with the substrate. The centrifugal force ($F = m\omega^2R$) applied to the droplet was calculated to be around 12 mN (Figure 4.4.(c)). The adhesion strength of the EG drop to the steel substrate normalized by the contact area of 0.2 mm^2 was approximately 60 kPa . The stability of EG drops on the substrate suggests that for real applications, the spray may be applied conveniently anytime before loading oil sands to the truck.

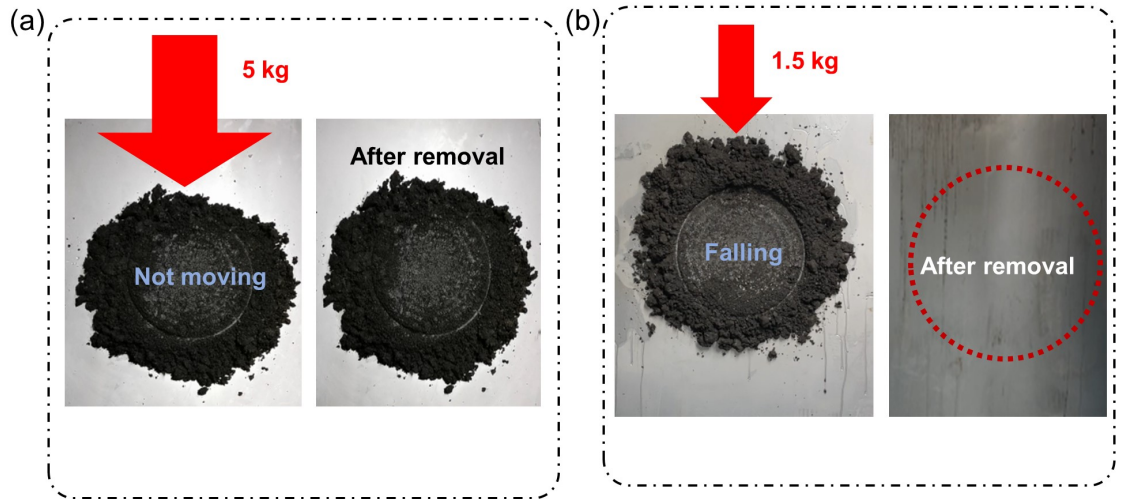


Figure 4.5: Effects of EG spray (EG:water = 2:1) on reducing oil sands adhesion at large scale. Snapshots were taken from the video recording of the removing process in the walk-in freezer after the oil sands were frozen at $-18 \text{ }^\circ\text{C}$ for 2 *hr*. (a) - Without anti-freezing liquid spray, oil sands could not be removed with 5 kg of load; (b) - with anti-freezing liquid spray, oil sands could be easily removed with 1.5 kg of load. No stain was observed after swiping with acetone in the freezer.

The anti-fouling performance of anti-freezing liquid was also tested at large scale as shown in Figure 4.5. Detailed testing procedure is discussed in the Experimental section. For substrates without anti-freezing coating, oil sands could not be removed with $\sim 5 \text{ kg}$ of load nor by swiping with acetone at $-18 \text{ }^\circ\text{C}$. In contrast, for the substrates with EG coating (Figure 4.5.(b)), the frozen oil sands can be easily removed

with ~ 1.5 kg of load on the oil sands sample. Only slight stain of bitumen was left after oil sand fell off the substrate. The bitumen stain can be cleaned with acetone swipe in the freezer, and the steel substrate after cleaning was almost as clean as the condition before the test. The result indicates that by spray coating anti-freezing liquid onto steel substrate, it is possible to remove the oil sands carryover, and thus save the time and energy consumption from the traditional shoveling method.

The cost of the spray (EG:water = 2:1) is estimated by multiplying the price per volume of the spray with the estimated total volume of spray on the truck for each year. From the photo shown in Figure 4.4, it is reasonable to assume the spray on the steel substrate is a layer of uniform coating with a thickness of ~ 100 μm . The price of ethylene glycol on the market is $\sim 1,000$ CAD/ m^3 . Considering that the total area of the truck bed and canopy is around 75 m^2 , the cost for each truck for each run will be only 0.5 CAD. From the field data, each truck will take around $6,000$ runs to transport the oil sands from the mining spot in each winter, and there are less than 100 trucks working on the field at the same time. Assuming that the spray is required after each run of transportation, the total cost of the spray for one fleet each year will be ~ 0.3 million CAD, which is much less compared with the additional cost from the surface fouling (~ 8 million CAD).

4.4 Conclusions

In this chapter, we showed that the adhesion of frozen oil sand was affected by the substrate type as well as the load applied to the sand. Ice adhesion strength on all six substrates in our experiments was found to correlate linearly with the adhesion strength of frozen oil sands. Higher load was found to increase the adhesion strength, possibly due to increased contact area with water in compact matrix of oil sands. Up to a plateau load (i.e., 450 kPa), additional load could not increase the adhesion strength any further. The maximum adhesion strength may be due to the limit of particle packing of oil sands. Anti-freezing liquid was proved to effectively reduce

the adhesion strength for oil sands under the freezing point of water. Applying anti-freezing liquid was effective in reducing adhesion on all tested substrates including pristine steel and oil sands-fouled substrates. The method of spray-coating of anti-freezing liquid may provide a solution for eliminating carryover in transport of oil sands in cold regions, as the method is time effective and easy to implement with potential applications for autonomous mining.

Chapter 5

Conclusions & Future Work

5.1 Main results and contributions

In Chapter 3, we found that water content is critical for the adhesion of oil sands (a complex granular matter) at low temperature. The images from our micro-CT measurements showed that the air pockets in oil sands were filled with interstitial water, which formed capillary bridges with the substrate. The adhesion strength of oil sands increased linearly on steel and rubber substrates with increase in the water content, and also with the degree of supercooling within a short freezing time. Fouling from bitumen or asphaltene layer on the surface aggravated the adhesion of oil sands on steel. Based on the significant impact from ice formation, we demonstrated that the effective approach to reducing the adhesion of oil sands is to spray anti-freezing liquid on the substrate.

While in Chapter 4, we showed that the adhesion of frozen oil sand was affected by the substrate type as well as the load applied to the sand. Ice adhesion strength on all six substrates in our experiments was found to correlate linearly with the adhesion strength of frozen oil sands. Higher load was found to increase the adhesion strength, possibly due to increased contact area with water in compact matrix of oil sands. Up to a plateau load (i.e., 450 kPa), additional load could not increase the adhesion strength any further. The maximum adhesion strength may be due to the limit of particle packing of oil sands. Anti-freezing liquid was proved to effectively reduce

the adhesion strength for oil sands under the freezing point of water. Applying anti-freezing liquid was effective in reducing adhesion on all tested substrates including pristine steel and oil sands-fouled substrates. The method of spray-coating of anti-freezing liquid may provide a solution for eliminating carryover in transport of oil sands in cold regions, as the method is time effective and easy to implement with potential applications for autonomous mining.

The findings from this thesis work may lead to promising solutions to prevent the accumulation of oil sands on truck surfaces at low temperature. The fundamental understanding of the adhesion may be applicable to the adhesion of other frozen granular matters on solid substrates. Based on the solution of anti-freezing liquid spray coating provided in this work, the efficiency of transportation of oil sands at low temperatures could increase. Meanwhile, the high cost from the labor and energy intensive cleaning process for oil sands stain on surfaces may be reduced, which might be profitable for the oil industry in many aspects.

5.2 Future Work

The work from this thesis was based on a real issue of oil sands adhere strongly to the surface of truck bed and canopy at low temperature in the oil industry. The research work drove us to explore the contribution of the components of oil sands interacting with the solid substrate at the interface on the adhesion strength and we determined the main contribution was from the freezing of water, and the ice adhesion strength on a solid substrate was found to have a linear relationship with the oil sands adhesion strength. With this understanding, we came up with a strategy of spray coating of anti-freezing liquid and it was tested to perform well at both lab and industrial scale. To further explore the phenomenon of the adhesion of frozen granular matter on solid substrates and develop approaches to mitigate the adhesion, there are several technical and fundamental issues deserve a deeper investigation.

1. Evaluate the effect of surface roughness on steel substrate. In this thesis work, the stainless steel substrate was just used as received without a control of the surface roughness. From the oil sands adhesion strength measurement, we found a stronger adhesion on the bitumen/asphaltene coating compared with pristine steel, demonstrating a possibility of the influence from surface roughness. Polishing the steel substrate to certain surface finishes would be a solution to control the surface roughness.
2. Characterize the water freezing process in oil sands granular matrix in-situ. The oil sands sample was characterized by micro-CT imaging system under ambient condition. Observing the freezing process of water bridges between the granular matrix would help the understanding of the adhesion of frozen granular matter, and possibly help with finding other solutions. Possible tools to observe the ice formation in granular matrix are differential scanning calorimetry (DSC), nuclear magnetic resonance (NMR), and X-ray diffraction (XRD). In the appendix, we will demonstrate the process and results of DSC test for oil sands sample with 2 water content levels as an example.
3. Fabricate artificial water-wet granular matrix to study the influence from the composition on the adhesion strength of frozen granular matter. In this thesis work, the type of granular matrix was only oil sands, which was restricted by the time-sensitive issue from the oil industry. To better investigate the adhesion of frozen granular matter, making artificial granular system should help with separating the influence from each component, like the size of the solid particles, metal salts concentration in water, and the type of miscible/immiscible liquid added into the system. In the appendix, we will demonstrate the process and results of adhesion strength measurement of a water-wet sand system as an example.
4. Test the performance of spraying of hydrophobic PDMS-based coating on steel

substrates in reducing the adhesion strength of frozen oil sands. The oil sands adhesion strength was determined to have a linear relationship with ice adhesion strength on the substrates. Hydrophobic coatings naturally has a lower ice adhesion strength, and spraying method is favorable for large scale industrial applications. With the self-healing property developed by researchers, PDMS-based sprayable coating is a type of material showing good potential to mitigate frozen oil sands in the oil industry. Compared with anti-freezing liquid spray, which required spraying for each run, the coating could sustain for a longer time with the load-unload cycles of oil sands.

Bibliography

- [1] J. Bockheim, “Ice core and ice cement effects on soil development, eastern wright valley, antarctica,” *New Zealand Journal of Geology and Geophysics*, vol. 22, no. 4, pp. 487–493, 1979.
- [2] R. George, “Freezing proceseses used in the food industry,” *Trends in Food Science & Technology*, vol. 4, no. 5, pp. 134–138, 1993.
- [3] H. Kiani and D.-W. Sun, “Water crystallization and its importance to freezing of foods: A review,” *Trends in Food Science & Technology*, vol. 22, no. 8, pp. 407–426, 2011.
- [4] T. Kang, Y. You, and S. Jun, “Supercooling preservation technology in food and biological samples: A review focused on electric and magnetic field applications,” *Food science and biotechnology*, vol. 29, no. 3, pp. 303–321, 2020.
- [5] L. Qian and H. Zhang, “Controlled freezing and freeze drying: A versatile route for porous and micro-/nano-structured materials,” *Journal of Chemical Technology & Biotechnology*, vol. 86, no. 2, pp. 172–184, 2011.
- [6] B. Ke, K. Zhou, C. Xu, H. Deng, J. Li, and F. Bin, “Dynamic mechanical property deterioration model of sandstone caused by freeze–thaw weathering,” *Rock Mechanics and Rock Engineering*, vol. 51, no. 9, pp. 2791–2804, 2018.
- [7] S Bolliger, H Wildmoser, H. Goff, and B. Tharp, “Relationships between ice cream mix viscoelasticity and ice crystal growth in ice cream,” *International Dairy Journal*, vol. 10, no. 11, pp. 791–797, 2000.
- [8] L. He, X. Li, G. Wu, F. Lin, and H. Sui, “Distribution of saturates, aromatics, resins, and asphaltenes fractions in the bituminous layer of athabasca oil sands,” *Energy & fuels*, vol. 27, no. 8, pp. 4677–4683, 2013.
- [9] F. Nie, D. He, J. Guan, X. Li, Y. Hong, L. Wang, H. Zheng, and Q. Zhang, “Oil sand pyrolysis: Evolution of volatiles and contributions from mineral, bitumen, maltene, and sara fractions,” *Fuel*, vol. 224, pp. 726–739, 2018.
- [10] L. G. Hepler and C. Hsi, “Aostra technical handbook on oil sands, bitumens and heavy oils,” 1989.
- [11] A. Hooshiar, P. Uhlik, Q. Liu, T. H. Etsell, and D. G. Ivey, “Clay minerals in nonaqueous extraction of bitumen from alberta oil sands: Part 1. nonaqueous extraction procedure,” *Fuel Process. Technol.*, vol. 94, no. 1, pp. 80–85, 2012.

- [12] H. Nikakhtari, S. Wolf, P. Choi, Q. Liu, and M. R. Gray, "Migration of fine solids into product bitumen from solvent extraction of alberta oilsands," *Energy & fuels*, vol. 28, no. 5, pp. 2925–2932, 2014.
- [13] W. Bascom, R. Cottingham, and C. Singleterry, "Ice adhesion to hydrophilic and hydrophobic surfaces," *The Journal of Adhesion*, vol. 1, no. 4, pp. 246–263, 1969.
- [14] I. A. Ryzhkin and V. F. Petrenko, "Physical mechanisms responsible for ice adhesion," *The Journal of Physical Chemistry B*, vol. 101, no. 32, pp. 6267–6270, 1997.
- [15] S. Rønneberg, J. He, and Z. Zhang, "The need for standards in low ice adhesion surface research: A critical review," *Journal of Adhesion Science and Technology*, vol. 34, no. 3, pp. 319–347, 2020.
- [16] A. J. Meuler, J. D. Smith, K. K. Varanasi, J. M. Mabry, G. H. McKinley, and R. E. Cohen, "Relationships between water wettability and ice adhesion," *ACS applied materials & interfaces*, vol. 2, no. 11, pp. 3100–3110, 2010.
- [17] Y. H. Yeong, A. Millionis, E. Loth, J. Sokhey, and A. Lambourne, "Atmospheric ice adhesion on water-repellent coatings: Wetting and surface topology effects," *Langmuir*, vol. 31, no. 48, pp. 13 107–13 116, 2015.
- [18] A. Dotan, H Dodiuk, C Laforte, and S Kenig, "The relationship between water wetting and ice adhesion," *Journal of Adhesion Science and Technology*, vol. 23, no. 15, pp. 1907–1915, 2009.
- [19] M. Nosonovsky and V. Hejazi, "Why superhydrophobic surfaces are not always icephobic," *ACS nano*, vol. 6, no. 10, pp. 8488–8491, 2012.
- [20] Q. Fu, X. Wu, D. Kumar, J. W. Ho, P. D. Kanhere, N. Srikanth, E. Liu, P. Wilson, and Z. Chen, "Development of sol–gel icephobic coatings: Effect of surface roughness and surface energy," *ACS applied materials & interfaces*, vol. 6, no. 23, pp. 20 685–20 692, 2014.
- [21] M. R. Kasaai and M. Farzaneh, "Evaluation of mechanisms of ice adhesion on power network equipment," in *International Conference on Offshore Mechanics and Arctic Engineering*, vol. 37459, 2004, pp. 927–932.
- [22] M. Hassan, H. Lee, and S. Lim, "The variation of ice adhesion strength with substrate surface roughness," *Measurement Science and Technology*, vol. 21, no. 7, p. 075 701, 2010.
- [23] J. Chen, J. Liu, M. He, K. Li, D. Cui, Q. Zhang, X. Zeng, Y. Zhang, J. Wang, and Y. Song, "Superhydrophobic surfaces cannot reduce ice adhesion," *Applied Physics Letters*, vol. 101, no. 11, p. 111 603, 2012.
- [24] T. Strobl, D. M. Raps, and M. Hornung, "Evaluation of roughness effects on ice adhesion," in *5th AIAA Atmospheric and Space Environments Conference*, 2013, p. 2547.

- [25] E. J. Y. Ling, V. Uong, J.-S. Renault-Crispo, A.-M. Kietzig, and P. Servio, “Reducing ice adhesion on nonsmooth metallic surfaces: Wettability and topography effects,” *ACS applied materials & interfaces*, vol. 8, no. 13, pp. 8789–8800, 2016.
- [26] R. Raj, R. Enright, Y. Zhu, S. Adera, and E. N. Wang, “Unified model for contact angle hysteresis on heterogeneous and superhydrophobic surfaces,” *Langmuir*, vol. 28, no. 45, pp. 15 777–15 788, 2012.
- [27] J. W. Drelich, “Contact angles: From past mistakes to new developments through liquid-solid adhesion measurements,” *Advances in colloid and interface science*, vol. 267, pp. 1–14, 2019.
- [28] J. Wang, Y. Wu, Y. Cao, G. Li, and Y. Liao, “Influence of surface roughness on contact angle hysteresis and spreading work,” *Colloid and Polymer Science*, vol. 298, pp. 1107–1112, 2020.
- [29] H. A. Stone, “Ice-phobic surfaces that are wet,” *Acs Nano*, vol. 6, no. 8, pp. 6536–6540, 2012.
- [30] S. Kulinich and M Farzaneh, “Ice adhesion on super-hydrophobic surfaces,” *Applied Surface Science*, vol. 255, no. 18, pp. 8153–8157, 2009.
- [31] J. N. Israelachvili, *Intermolecular and surface forces*. Academic press, 2011.
- [32] P. Oksanen, “Friction and adhesion of ice,” 1983.
- [33] G. Fortin and J. Perron, “Ice adhesion models to predict shear stress at shedding,” *Journal of adhesion science and technology*, vol. 26, no. 4-5, pp. 523–553, 2012.
- [34] V. F. Petrenko and I. A. Ryzhkin, “Surface states of charge carriers and electrical properties of the surface layer of ice,” *The Journal of Physical Chemistry B*, vol. 101, no. 32, pp. 6285–6289, 1997.
- [35] S. Xiao, J. He, and Z. Zhang, “Modeling nanoscale ice adhesion,” *Acta Mechanica Solida Sinica*, vol. 30, no. 3, pp. 224–226, 2017.
- [36] V. F. Petrenko and S Peng, “Reduction of ice adhesion to metal by using self-assembling monolayers (sams),” *Canadian journal of physics*, vol. 81, no. 1-2, pp. 387–393, 2003.
- [37] K. Matsumoto, D. Tsubaki, K. Sekine, H. Kubota, K. Minamiya, and S. Yamanaoka, “Influences of number of hydroxyl groups and cooling solid surface temperature on ice adhesion force,” *International Journal of Refrigeration*, vol. 75, pp. 322–330, 2017.
- [38] L. Wilen, J. Wettlaufer, M Elbaum, and M Schick, “Dispersion-force effects in interfacial premelting of ice,” *Physical Review B*, vol. 52, no. 16, p. 12 426, 1995.
- [39] R. Menini and M. Farzaneh, “Advanced icephobic coatings,” *Journal of adhesion science and technology*, vol. 25, no. 9, pp. 971–992, 2011.

- [40] K. Matsumoto, K. Minamiya, H. Kubota, and K. Sekine, “Active control of ice adhesion force to copper surface by varying surfactant concentrations,” *International Journal of Refrigeration*, vol. 76, pp. 252–260, 2017.
- [41] K. Matsumoto, K. Minamiya, J. Sakamoto, J. Ueda, K. Ehara, and S. Yamanaka, “Temperature-dependency on adhesion force of ice made from surfactant–pure water mixture to copper surface,” *International Journal of Refrigeration*, vol. 79, pp. 39–48, 2017.
- [42] J. A. Elliott, “Surface thermodynamics at the nanoscale,” *The Journal of Chemical Physics*, vol. 154, no. 19, p. 190 901, 2021.
- [43] J. Blachere and J. Young, “The freezing point of water in porous glass,” *Journal of the American Ceramic Society*, vol. 55, no. 6, pp. 306–308, 1972.
- [44] N. Mitarai and F. Nori, “Wet granular materials,” *Adv. Phys.*, vol. 55, no. 1-2, pp. 1–45, 2006.
- [45] Z. He, S. Xiao, H. Gao, J. He, and Z. Zhang, “Multiscale crack initiator promoted super-low ice adhesion surfaces,” *Soft Matter*, vol. 13, no. 37, pp. 6562–6568, 2017.
- [46] Z. He, Y. Zhuo, J. He, and Z. Zhang, “Design and preparation of sandwich-like polydimethylsiloxane (pdms) sponges with super-low ice adhesion,” *Soft Matter*, vol. 14, no. 23, pp. 4846–4851, 2018.
- [47] Y. H. Yeong, C. Wang, K. J. Wynne, and M. C. Gupta, “Oil-infused superhydrophobic silicone material for low ice adhesion with long-term infusion stability,” *ACS Appl. Mater. Interfaces*, vol. 8, no. 46, pp. 32 050–32 059, 2016.
- [48] C. Wang, T. Fuller, W. Zhang, and K. J. Wynne, “Thickness dependence of ice removal stress for a polydimethylsiloxane nanocomposite: Sylgard 184,” *Langmuir*, vol. 30, no. 43, pp. 12 819–12 826, 2014.
- [49] D. L. Beemer, W. Wang, and A. K. Kota, “Durable gels with ultra-low adhesion to ice,” *J. Mater. Chem. A*, vol. 4, no. 47, pp. 18 253–18 258, 2016.
- [50] K. Khanafer, A. Duprey, M. Schlicht, and R. Berguer, “Effects of strain rate, mixing ratio, and stress-strain definition on the mechanical behavior of the polydimethylsiloxane (pdms) material as related to its biological applications,” *Biomed. Microdevices*, pp. 503–508, 2021.
- [51] K. Golovin, S. P. Kobaku, D. H. Lee, E. T. DiLoreto, J. M. Mabry, and A. Tuteja, “Designing durable icephobic surfaces,” *Science advances*, vol. 2, no. 3, e1501496, 2016.
- [52] Y. Liu, L. Ma, W. Wang, A. K. Kota, and H. Hu, “An experimental study on soft pdms materials for aircraft icing mitigation,” *Appl. Surf. Sci.*, vol. 447, pp. 599–609, 2018.
- [53] K Kendall, “The adhesion and surface energy of elastic solids,” *Journal of Physics D: Applied Physics*, vol. 4, no. 8, p. 1186, 1971.

- [54] L. Zhu, J. Xue, Y. Wang, Q. Chen, J. Ding, and Q. Wang, "Ice-phobic coatings based on silicon-oil-infused polydimethylsiloxane," *ACS applied materials & interfaces*, vol. 5, no. 10, pp. 4053–4062, 2013.
- [55] Y. Wang, X. Yao, J. Chen, Z. He, J. Liu, Q. Li, J. Wang, and L. Jiang, "Organogel as durable anti-icing coatings," *Science China Materials*, vol. 58, no. 7, pp. 559–565, 2015.
- [56] Y. Zhuo, S. Xiao, A. Amirfazli, J. He, and Z. Zhang, "Polysiloxane as icephobic materials—the past, present and the future," *Chemical Engineering Journal*, p. 127 088, 2020.
- [57] J. Chen, Z. Luo, Q. Fan, J. Lv, and J. Wang, "Anti-ice coating inspired by ice skating," *Small*, vol. 10, no. 22, pp. 4693–4699, 2014.
- [58] J. Chen, R. Dou, D. Cui, Q. Zhang, Y. Zhang, F. Xu, X. Zhou, J. Wang, Y. Song, and L. Jiang, "Robust prototypical anti-icing coatings with a self-lubricating liquid water layer between ice and substrate," *ACS applied materials & interfaces*, vol. 5, no. 10, pp. 4026–4030, 2013.
- [59] R. Dou, J. Chen, Y. Zhang, X. Wang, D. Cui, Y. Song, L. Jiang, and J. Wang, "Anti-icing coating with an aqueous lubricating layer," *ACS applied materials & interfaces*, vol. 6, no. 10, pp. 6998–7003, 2014.
- [60] C. Tao, S. Bai, X. Li, C. Li, L. Ren, Y. Zhao, and X. Yuan, "Formation of zwitterionic coatings with an aqueous lubricating layer for antifogging/anti-icing applications," *Progress in Organic Coatings*, vol. 115, pp. 56–64, 2018.
- [61] D. Chen, M. D. Gelenter, M. Hong, R. E. Cohen, and G. H. McKinley, "Ice-phobic surfaces induced by interfacial nonfrozen water," *ACS applied materials & interfaces*, vol. 9, no. 4, pp. 4202–4214, 2017.
- [62] B. Yi, P. Liu, C. Hou, C. Cao, J. Zhang, H. Sun, and X. Yao, "Dual-cross-linked supramolecular polysiloxanes for mechanically tunable, damage-healable and oil-repellent polymeric coatings," *ACS applied materials & interfaces*, vol. 11, no. 50, pp. 47 382–47 389, 2019.
- [63] C. Cao, B. Yi, J. Zhang, C. Hou, Z. Wang, G. Lu, X. Huang, and X. Yao, "Sprayable superhydrophobic coating with high processibility and rapid damage-healing nature," *Chem. Engr. J.*, vol. 392, p. 124 834, 2020.
- [64] J. J. Adams, "Asphaltene adsorption, a literature review," *Energy & Fuels*, vol. 28, no. 5, pp. 2831–2856, 2014.
- [65] Y. Shen, Y. Wu, J. Tao, C. Zhu, H. Chen, Z. Wu, and Y. Xie, "Spraying fabrication of durable and transparent coatings for anti-icing application: Dynamic water repellency, icing delay, and ice adhesion," *ACS applied materials & interfaces*, vol. 11, no. 3, pp. 3590–3598, 2018.
- [66] B. F. Blackwell, W. Gill, K. J. Dowding, and R. G. Easterling, "Uncertainty estimation in the determination of thermal conductivity of 304 stainless steel," Sandia National Labs., Albuquerque, NM (US); Sandia National Labs . . . , Tech. Rep., 2000.

- [67] R. S. Graves, T. G. Kollie, D. L. McElroy, and K. E. Gilchrist, “The thermal conductivity of AISI 304L stainless steel,” *International journal of thermo-physics*, vol. 12, no. 2, pp. 409–415, 1991, Publisher: Springer.
- [68] T Bhowmick and S Pattanayak, “Thermal conductivity, heat capacity and diffusivity of rubbers from 60 to 300 k,” *Cryogenics*, vol. 30, no. 2, pp. 116–121, 1990.
- [69] B Pinedo, M. Hadfield, I. Tzanakis, M Conte, and M Anand, “Thermal analysis and tribological investigation on tpu and nbr elastomers applied to sealing applications,” *Tribology International*, vol. 127, pp. 24–36, 2018.
- [70] J. Bulmer and J Starr, “Syncrude analytical methods for oil sand and bitumen processing,” 1979.
- [71] A. Hakimian, S. Nazifi, and H. Ghasemi, “Metrology of ice adhesion,” *Ice Adhesion: Mechanism, Measurement and Mitigation*, pp. 217–236, 2020.
- [72] K. Mirshahidi, K. A. Zarasvand, W. Luo, and K. Golovin, “A high throughput tensile ice adhesion measurement system,” *HardwareX*, vol. 8, e00146, 2020.
- [73] L.-O. Andersson, C.-G. Golander, and S. Persson, “Ice adhesion to rubber materials,” *Journal of Adhesion science and technology*, vol. 8, no. 2, pp. 117–132, 1994.
- [74] C. Laforte and A. Beisswenger, “Icephobic material centrifuge adhesion test,” in *Proceedings of the 11th International Workshop on Atmospheric Icing of Structures, IWAIS, Montreal, QC, Canada*, 2005, pp. 12–16.
- [75] S. Rønneberg, C. Laforte, C. Volat, J. He, and Z. Zhang, “The effect of ice type on ice adhesion,” *AIP Advances*, vol. 9, no. 5, p. 055304, 2019.
- [76] M. R. Kasaai and M. Farzaneh, “A critical review of evaluation methods of ice adhesion strength on the surface of materials,” in *International Conference on Offshore Mechanics and Arctic Engineering*, vol. 37459, 2004, pp. 919–926.
- [77] A. Work and Y. Lian, “A critical review of the measurement of ice adhesion to solid substrates,” *Progress in Aerospace Sciences*, vol. 98, pp. 1–26, 2018.
- [78] S. Ozbay and H. Y. Erbil, “Ice accretion by spraying supercooled droplets is not dependent on wettability and surface free energy of substrates,” *Colloids and Surfaces A: Physicochemical and Engineering Aspects*, vol. 504, pp. 210–218, 2016.
- [79] R. M. Fillion, A. Riahi, and A Edrisy, “Design factors for reducing ice adhesion,” *Journal of adhesion science and technology*, vol. 31, no. 21, pp. 2271–2284, 2017.
- [80] D. Wang, Q. Sun, M. J. Hokkanen, C. Zhang, F.-Y. Lin, Q. Liu, S.-P. Zhu, T. Zhou, Q. Chang, B. He, *et al.*, “Design of robust superhydrophobic surfaces,” *Nature*, vol. 582, no. 7810, pp. 55–59, 2020.
- [81] H. Ledbetter, N. Frederick, and M. Austin, “Elastic-constant variability in stainless-steel 304,” *Journal of Applied Physics*, vol. 51, no. 1, pp. 305–309, 1980.

- [82] A Zikin, I Hussainova, C Katsich, E Badisch, and C Tomastik, “Advanced chromium carbide-based hardfacings,” *Surface and Coatings Technology*, vol. 206, no. 19-20, pp. 4270–4278, 2012.
- [83] X. Wu, X. Zhao, J. W. C. Ho, and Z. Chen, “Design and durability study of environmental-friendly room-temperature processable icephobic coatings,” *Chemical Engineering Journal*, vol. 355, pp. 901–909, 2019.
- [84] M. Bouteau, S. Cantin, O. Fichet, F. Perrot, and D. Teyssié, “Contribution toward comprehension of contact angle values on single polydimethylsiloxane and poly (ethylene oxide) polymer networks,” *Langmuir*, vol. 26, no. 22, pp. 17 427–17 434, 2010.
- [85] Q. Yang, J. B. You, B. Tian, S. Sun, D. Daniel, Q. Liu, and X. Zhang, “Water-mediated adhesion of oil sands on solid surfaces at low temperature,” 2021.
- [86] H. Mochinaga, S Onozuka, F. Kono, T. Ogawa, A. Takahashi, and T. Torigoe, “Properties of oil sands and bitumen in athabasca,” in *The Canadian Society of Exploration Geologists CSPG–CSEG–CWLS Convention*, 2006, pp. 39–44.
- [87] J. Czarnecki, B. Radoev, L. L. Schramm, and R. Slavchev, “On the nature of athabasca oil sands,” *Advances in Colloid and Interface Science*, vol. 114, pp. 53–60, 2005.
- [88] D. Kashchiev, *Nucleation*. Elsevier, 2000.
- [89] N. Maeda, “Brief overview of ice nucleation,” *Molecules*, vol. 26, no. 2, p. 392, 2021.
- [90] P. G. Nutting, “Physical analysis of oil sands,” *AAPG Bulletin*, vol. 14, no. 10, pp. 1337–1349, 1930.
- [91] D. H. Doan, P. Delage, J. F. Nauroy, A. M. Tang, and S. Youssef, “Microstructural characterization of a canadian oil sand,” *Canadian Geotechnical Journal*, vol. 49, no. 10, pp. 1212–1220, 2012.
- [92] G. D. Mossop, “Geology of the athabasca oil sands,” *Science*, vol. 207, no. 4427, pp. 145–152, 1980.
- [93] M. B. Dusseault and N. R. Morgenstern, “Shear strength of athabasca oil sands,” *Canadian Geotechnical Journal*, vol. 15, no. 2, pp. 216–238, 1978.
- [94] C Bacher, P. Olsen, P Bertelsen, and J. Sonnergaard, “Compressibility and compactibility of granules produced by wet and dry granulation,” *International journal of pharmaceutics*, vol. 358, no. 1-2, pp. 69–74, 2008.
- [95] L. Makkonen, “Ice adhesion—theory, measurements and countermeasures,” *Journal of Adhesion Science and Technology*, vol. 26, no. 4-5, pp. 413–445, 2012.
- [96] H. Memon, J. Liu, D. S. De Focatiis, K.-s. Choi, and X. Hou, “Intrinsic dependence of ice adhesion strength on surface roughness,” *Surface and Coatings Technology*, vol. 385, p. 125 382, 2020.

- [97] E. M. Schulson, "The structure and mechanical behavior of ice," *Jom*, vol. 51, no. 2, pp. 21–27, 1999.
- [98] W. Meng and Y. Guo, "Experimental study on mechanical properties of ice," in *Proceedings of the AASRI International Conference on Industrial Electronics and Applications (IEA2015)*, London UK, 2015, pp. 192–196.
- [99] L. Fu, G. Zhang, J. Ge, K. Liao, Y. He, X. Wang, and H. Li, "Study on dual-frequency ultrasounds assisted surfactant extraction of oil sands," *Fuel Processing Technology*, vol. 167, pp. 146–152, 2017.
- [100] X. Zhao, "Novel green processing of oil sands: From extraction of bitumen to treatment of byproducts," PhD thesis, The University of Utah, 2018.
- [101] J. M. Hollis, F. J. Lovas, P. R. Jewell, and L. Coudert, "Interstellar antifreeze: Ethylene glycol," *The Astrophysical Journal Letters*, vol. 571, no. 1, p. L59, 2002.
- [102] K. Bischoff, "Propylene glycol," *Small Animal Toxicology. St. Louis: Elsevier Saunders*, pp. 996–1001, 2006.

Appendix A: DSC result of oil sands sample

A.1 Procedure of DSC tests

For DSC tests, we used oil sands with 2 water content levels: 4 wt% and 10 wt%. Oil sands sample prepared as described in Chapter 3 was defrost in sealed plastic bags under ambient condition for 3 *hr*. About 2 *mg* of the oil sands sample was transferred into the Hermetic aluminum sample pan and sealed by a lid. After mounting the sample pan onto the sample stage of the DSC analyze system (DSC-Q1000, TA, USA). The target temperature of the sample was first stabilized at 0 °C for 3 *min*, and decreased to -25 °C with a cooling rate of 5 °C/*min*.

A.2 Results of DSC tests

From the figure, we demonstrated the heat flow curve during the freezing of the oil sands sample from 0 °C to -25 °C. From the curve, we observed a peak for sand-water sample with 10 wt% of water contents, which did not appear for the sample with 4 wt% of water contents. Since the positive direction of the heat flow axis denotes the release of heat from the sample to the surroundings, we could know that the peak shown in the figure represents the process of water nucleation (an exothermic process). The temperature where we observed the peak was -6.7 °C, which is lower than the ice point of bulk water (0 °C). This could be possibly explained by the combining energy between water and the sand particles that prevented water from nucleating into ice at the normal ice point. The possible reason for us not seeing a peak for

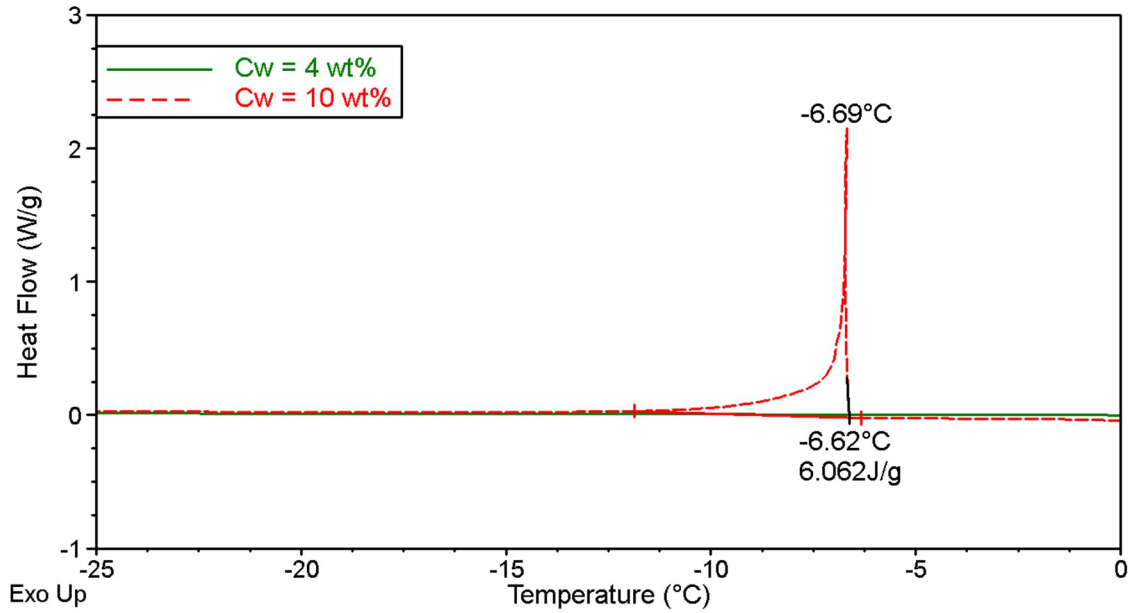


Figure A.1: DSC result of oil sands sample with 4 and 10 wt% of water. The positive direction of heat flow axis denotes releasing heat from the sample to the surroundings.

sands sample with 4 wt% of water contents could be due to the water distribution in granular matrix. Small amount of water (4 wt%) tended to wrap the sand particles instead of generating water bridges in between the particles as in samples with higher water content (10 wt%). Because water was in close contact with the sands in the sample with 4 wt% of water contents, the freezing point of water was subsequently suppressed to lower than -25°C without contacting a solid substrate.

Appendix B: Influence of particle size on adhesion force of water-wet sands

B.1 Preparation of sample and procedure of adhesion force measurements

To prepare water-wet sand samples with controlled water weight percentage (C_w), a certain volume of deionized water was added with micro-pipettes and the sand-water mixture was homogenized manually. To evaluate the effect of particle size, 3 types of sand samples with diversified diameter ranges were used: $210 \mu m - 420 \mu m$, $149 \mu m - 210 \mu m$, and $74 \mu m$. To prevent evaporation of water, the prepared samples with certain water contents were sealed in plastic bags till the measurements.

The measurement of adhesion force of the wet sands samples was similar to the procedure of measuring the oil sands adhesion introduced in Chapter 3 and Chapter 4. In brief, about $0.3 g$ of the wet sands sample was filled in the sample holder placed on the steel substrate mounted to the Peltier stage. $30 kPa$ of load was placed onto the sample while freezing at $-10 \text{ }^\circ\text{C}$ for 15 min . After frozen, the load was removed and the sample was pushed away by the force gauge, measuring the detaching force from the substrate.

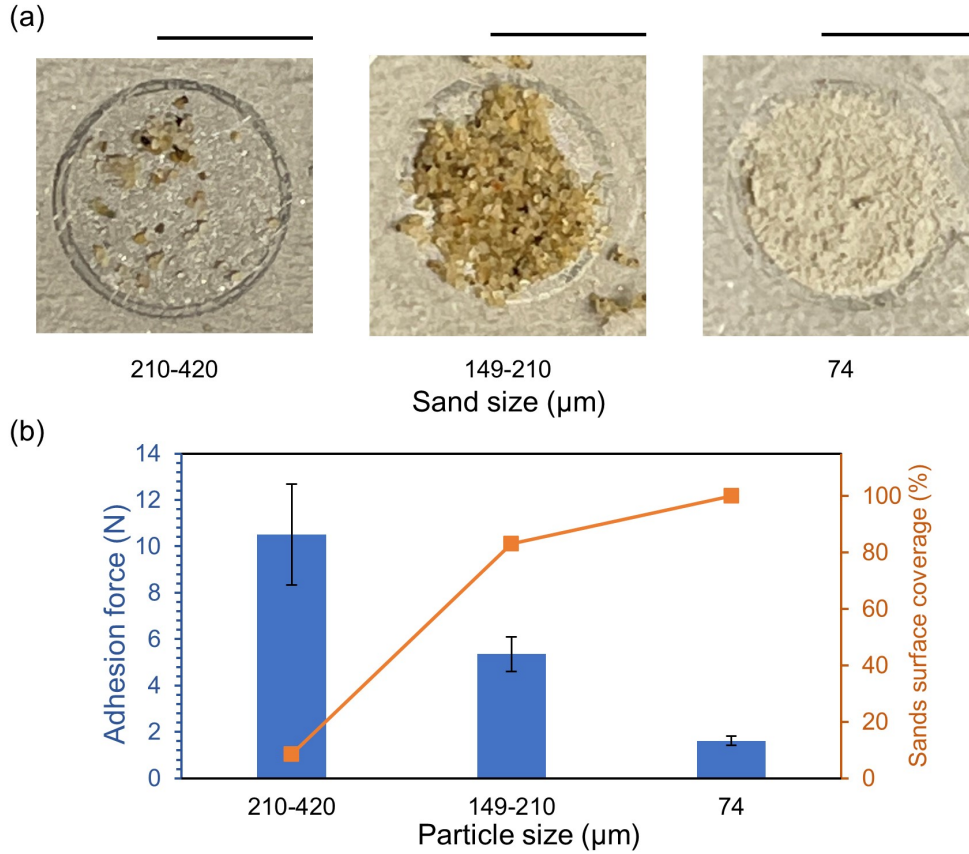


Figure B.1: (a) - Photos of the substrate after adhesion force measurement. Length of scale bar: 5 mm; (b) - Adhesion force of wet sands ($C_w = 4$ wt%) with 3 particle size distributions on steel substrate with 15 min of freezing under 60 kPa of load. Error bars are standard deviation of at least 3 repeated measurements.

B.2 Results of sand adhesion force measurements

In Figure B.1, we showed the adhesion force measured by our setup for wet sands ($C_w = 4$ wt%) with 3 sizes: 210-420 μm, 149-210 μm, and 74 μm. From Figure B.1.(a), we could see that for wet sands samples, there was residual sample left on the substrate after the majority of the sample detached by the pushing force. The sands residue indicated that the adhesion strength between the sample and the steel substrate was stronger than that between wet sands particles, which was not observed for oil sands samples. The possible mechanism of oil sands sample not leaving residue was that the bitumen content in oil sands served as a shield between water and the substrate. Thus the contact area of water was limited, and the adhesion strength of oil sands to

the substrate was decreased.

From Figure B.1.(b), we could see an obvious trend of adhesion force decreased with particle size from around 10 N for sands diameter of 210-420 μm to less than 2 N for sands diameter of 74 μm . The higher adhesion force for sands with larger diameter can be attributed to the less compact packing, which could provide larger area for water to form bridges. Assuming the ice adhesion strength between sands particles to be the same for all the wet sands samples, the larger ice coverage of the sands surface yields a stronger adhesion force. Also, from the trend of surface coverage of sands on the substrate we could see that for sands with smaller size, the surface area covered by residue sand is higher.